

Correlation effects in two-dimensional topological insulators

M Hohenadler and F F Assaad

Institut für Theoretische Physik und Astrophysik, Universität Würzburg,
Am Hubland, 97074 Würzburg, DE

E-mail: mhohenadler@physik.uni-wuerzburg.de

Abstract. Topological insulators have become one of the most active research areas in condensed matter physics. This article reviews progress on the topic of electronic correlations effects in the two-dimensional case, with a focus on systems with intrinsic spin-orbit coupling and numerical results. Topics addressed include an introduction to the noninteracting case, an overview of theoretical models, correlated topological band insulators, interaction-driven phase transitions, topological Mott insulators and fractional topological states, correlation effects on helical edge states, and topological invariants of interacting systems.

Contents

1	Introduction	2
2	Theoretical models	4
2.1	Kane-Mele-Hubbard model	4
2.2	Haldane-Hubbard model	5
2.3	Bernevig-Hughes-Zhang-Hubbard model	6
2.4	Sodium iridate model	6
2.5	Other models	7
3	Noninteracting quantum spin Hall insulator	7
4	Bulk correlation effects	10
4.1	Phases of the Kane-Mele-Hubbard model	11
4.2	Correlated topological band insulators	11
4.3	Interaction-driven phase transitions	12
4.3.1	Symmetry-breaking transitions	13
4.3.2	Symmetry-conserving transitions	15
4.4	Interaction-driven topological insulators	16
4.5	Fractional topological insulators	18
5	Edge correlation effects	19
5.1	Luttinger liquid description	19
5.2	Strongly correlated regime	22
6	Topological invariants of correlated systems	25
7	Conclusions and outlook	29

1. Introduction

The characterization of states of matter in terms of spontaneously broken symmetries and the corresponding order parameters, known as Ginzburg-Landau theory [1], is one of the most important concepts in condensed matter theory. Perhaps the best known and studied example is that of magnetic order, for instance originating from strong electronic interactions. Remarkably, there also exist insulating phases of matter which do not break any symmetries, yet are distinct from simple band insulators. The first such state to be discovered was the integer *quantum Hall state* of a two-dimensional electron gas in a strong magnetic field [2], see [3] for an introduction. Its quantized Hall conductivity (in two dimensions, conductance and conductivity are identical) can be explained by the existence of a topological invariant (the Chern number) calculated from a single-particle Hamiltonian [4–6]. Because this number cannot change under adiabatic transformations of the Hamiltonian, the integer quantum Hall state is topologically different from a trivial band insulator. In particular, a transition between these two states can only occur via a closing of the band gap. As a result, metallic states emerge at the edge of quantum Hall samples [7]. Moreover, while atomic insulators may be described as product states of completely local electronic wave functions, topological states show a distinct response to boundary conditions [8]. Haldane [9] showed that a quantum Hall state with broken time-reversal symmetry can not only be achieved with an external magnetic field, but also with a periodic magnetic flux.

Topological insulators (a name apparently first coined in [10]) represent another class of states that are topologically distinct from simple band insulators. They are symmetric under time reversal, and can therefore be realized experimentally without magnetic fields. Topological insulators were first discovered in a theoretical model for graphene [11, 12], in the context of the search for an intrinsic quantum spin Hall effect. Kane and Mele [11, 12] showed that the intrinsic spin-orbit coupling gives rise to an insulating state with a topological band structure, and a nonzero spin Hall response related to metallic edge states that are protected against perturbations by time-reversal symmetry. Topological insulators in three dimensions were predicted soon after [13], and are by now well confirmed by experiments [14]. Two-dimensional topological insulators, or *quantum spin Hall insulators*, have close conceptual relations to integer quantum Hall states: in the simplest case, the theoretical model of Kane and Mele [11, 12] is completely equivalent to two decoupled copies (with opposite chirality for the two spin directions) of the Haldane model for the integer quantum Hall effect [11].

While the spin-orbit gap in graphene is too small to permit experimental observation (about 10^{-3} meV, see for example [15]; an experimentally observable spin-orbit gap has been predicted for silicene [16], see [17–

19]) for experimental progress with this honeycomb material), the quantum spin Hall state has been observed in CdTe/HgTe/CdTe heterostructures [20–22]. As first predicted theoretically [23], the low-energy physics of this system is determined by the gap at the Γ point. If the HgTe quantum well has a thickness below a critical value d_c of 6.3 nm, the band structure is dominated by the surrounding CdTe layers, and the normal regime, with the s (Γ_6) bands lying energetically above the p (Γ_8) bands, is realized. If the thickness exceeds the critical value, the band structure becomes dominated by that of the quantum well, and band inversion takes place. Bernevig *et al* [23] predicted samples with such an inverted band structure to be quantum spin Hall insulators with a band gap of tens of meV, which was soon verified experimentally [20, 21].

In the absence of interactions, topological insulators can be understood in terms of single-particle Hamiltonians, allowing for a full classification based on time-reversal, particle-hole, and chiral symmetry [24–26]. Recently, an extension to include crystal symmetries has been given [27]. This review is primarily concerned with correlation effects, which have been explored in the context of topological insulators in several different settings. The most direct way to theoretically explore correlation effects is to consider the impact of electron-electron interactions on a noninteracting quantum spin Hall state by adding interactions to models with intrinsic spin-orbit coupling. Remarkably, some of these models permit the application of exact numerical methods. With regard to experiment, such studies are relevant for materials with significant spin-orbit and electron-electron interactions. This situation is expected to occur in, for example, the transition-metal oxide Na_2IrO_3 [28]. The interplay of strong correlations and spin-orbit coupling in this and other materials may allow for realizations of complex spin models [29–33] and hence may provide a route to quantum spin liquids [34].

Even in materials with rather weak intrinsic spin-orbit coupling, robust quantum spin Hall states can emerge from strong electronic correlations via a dynamically generated spin-orbit coupling that is the result of spontaneous symmetry breaking [35]. The resulting *topological Mott insulators*, states with a band gap generated by interactions and edge states protected by time-reversal symmetry, have so far been explored only at the mean-field level. The term topological Mott insulator is also used in the literature to refer to exotic states in which the interplay of spin-orbit coupling and electronic correlations leads to spin-charge separation, gapped charge excitations, and a topological band structure carried by low-energy spinon excitations [36]. A novel Mott state arising from strong spin-orbit interaction has been found experimentally in Sr_2IrO_4 [37, 38].

A third direction of research is concerned with fractional topological insulators. The fractional quantum Hall state is a famous example of a topological phase

emerging from strong electronic interactions (for a concise introduction see [3]). In the latter, strong repulsion among electrons occupying partially filled, flat Landau levels leads to intriguing insulating states with quasi-particle excitations that carry fractional charge and have fractional statistics. Fractional quantum Hall states have been a major research topic for several decades, with enormous progress in theory and experiment, and potential applications in quantum computing [3]. Remarkably, much of the physics of the fractional quantum Hall effect can in theory also exist in Chern insulators [39], described by models that break time-reversal symmetry but have zero net magnetic flux, and are hence similar in spirit to Haldane’s model for the integer quantum Hall effect [9]. Proposals for the experimental realization of fractional Chern insulators involve materials with flat bands that allow for an enhancement of electron-electron interactions [40]. In close analogy to the noninteracting case, *fractional quantum spin Hall insulators* can be constructed by, in the simplest case, combining two fractional quantum Hall states [41]. The theory of time-reversal invariant insulators with protected edge states is one of the most active current research areas (see section 4.5).

In the context of correlated electrons, the concept of topological order has yet another, important meaning. Quite generally, a topologically ordered state is robust with respect to adiabatic transformations of the Hamiltonian. In the case of the Z_2 topological insulators, as realized for example in the Kane-Mele model [11, 12], this robustness is mathematically expressed by a topological invariant. However, even in the presence of electron-electron interactions, this state—having its origin in a topological band structure—is adiabatically connected to a noninteracting band insulator. A classification of such states based on Chern-Simons theory has recently been given [42]. Topological band insulators are distinct from the class of topological states that emerge from interactions and are not adiabatically connected to a noninteracting state. A particularly fascinating example are quantum spin liquids, which are insulating states—arising from quantum fluctuations—that do not break any symmetries but have highly nontrivial correlations. For the latter, the term *topological order* implies [43] (i) the existence of a gap to excited states, (ii) a topological ground-state degeneracy in a periodic system (a torus geometry in two dimensions), and (iii) the existence of fractional quasi-particle excitations with Abelian or non-Abelian statistics. Whereas (i) is also typical of topological band insulators, (ii) and (iii) are not. On the other hand, fractional quantum Hall liquids and hence also fractional topological insulators possess topological order. An important recent development is the use of the concept of quantum entanglement to study and classify topological states [44]. Whereas topological insulators are characterized by short-range quantum entanglement and fall into the class of

symmetry-protected topological states (stable with respect to perturbations that do not break the symmetry that underlies the topological properties), fractional topological states and quantum spin liquids have long-range quantum entanglement [45]. Whereas any short-range entangled state can be transformed into a product state by means of *local unitary transformations*, such a transformation is not possible in the presence of long-range quantum entanglement [44]. A classification of topological states, including correlated states, can be obtained by considering local unitary transformations with different symmetries. For a more detailed discussion, see [44–49].

Three-dimensional topological insulators are realized by several different materials [14, 50, 51]. Strong correlation effects have been argued to play a role in SmB_6 (a potential topological Kondo insulator) [52, 53] and in actinide compounds such as AmN (identified as a Z_2 topological insulator in theoretical calculations) [54]. A candidate system for a topological Mott insulator is Sr_2IrO_4 [37, 38]. In contrast, experiments for the two-dimensional case are so far restricted to HgTe quantum wells [20–22], and do not reveal any substantial electronic correlation effects. Consequently, the study of correlated quantum spin Hall insulators has so far been a predominantly theoretical effort. The search for candidate condensed matter settings is guided by the fact that the spin-orbit coupling increases with the atomic number. For example, strong and comparable electron-electron and spin-orbit interactions are expected for Ir-based transition metal oxides [28], with numerical evidence for a strongly correlated quantum spin Hall state [28], and the possibility of a topological Mott insulator phase [36]. Another useful experimental setting are heterostructures of transition-metal oxides, for example a bilayer of LaNiO_3 sandwiched between LaAlO_3 layers [55]. Such structures provide substantial tunability [55, 56], and have been proposed to realize topological phases emerging from either intrinsic spin-orbit coupling [55], or from interaction-induced ordering of complex orbitals [57–60]. Interaction induced topological phases may also exist in stacked graphene [61, 62], whereas the intrinsic spin-orbit coupling may be sufficiently enhanced in decorated graphene [63] or in molecular graphene [64] to make a topological phase observable. Although concrete materials for fractional topological insulators have not yet been identified, several candidate systems for Chern insulators are known, see [40] and references therein. Cold atoms in optical lattices, or on atom chips, provide an alternative route toward correlated topological states. Using suitable artificial gauge fields [65], Z_2 topological insulators with tunable interactions may be realized [66, 67]. The use of Rydberg atoms has also been suggested to realize topological Mott insulators [68] and fractional quantum Hall states [69]. Finally, correlated topological states may also be engineered with photons in cavity arrays, see [70, 71].

Despite the rather short history of topological insula-

tors, the literature is remarkably rich. Given the background of the authors, this review aims at providing an overview of work on electronic correlation effects in two dimensions, with a focus on models with intrinsic spin-orbit coupling and numerical studies. It thereby complements earlier reviews by Hasan and Kane [50], Moore [72], and Qi and Zhang [14], but omits other fascinating topics such as three-dimensional topological insulators [14, 50, 51], topological Kondo insulators [52, 73, 74], or topological superconductors [14, 24, 25, 50]. For a self-contained presentation, it includes an introduction to noninteracting quantum spin Hall insulators using the example of the Kane-Mele model. The review is organized as follows. In section 2, the most widely used theoretical models are introduced. A discussion of noninteracting quantum spin Hall insulators is provided in section 3. Correlation effects on bulk properties are considered in section 4, whereas correlated helical edge states are the topic of section 5. The calculation of topological invariants for correlated systems is reviewed in section 6, and section 7 gives conclusions and an outlook.

2. Theoretical models

Since the proposal by Kane and Mele [11, 12], a number of theoretical models for the quantum Hall and spin Hall effect have been discovered. The general structure of such models and possible realizations in semiconductors were discussed, for example, in [75]. In many cases, spinless quantum Hall models can readily be generalized to describe time-reversal invariant quantum spin Hall states by introducing a spin-orbit gap with a spin-dependent sign. Here the emphasis is on some of the most popular models that support a topological state originating from spin-orbit coupling in the absence of electronic interactions. Overviews of theoretical models can also be found in [8, 76].

A common feature of the quantum spin Hall models considered here is that the Hamiltonians may be expressed in terms of 4×4 Dirac matrices [8, 11]. Given inversion symmetry, such a representation is particularly useful to determine the topological invariant in the absence of interactions [8, 11]. The corresponding matrix representations of the KM and the Bernevig-Hughes-Zhang (BHZ) model can be found in [8]. To study local, Hubbard-type interactions, and also for numerical methods, the tight-binding real-space representations are more appropriate.

Because of the topological character of the quantum spin Hall state, the details of the Hamiltonian play a minor role, and different models share similar low-energy physics. In particular, universal field theory descriptions can be obtained using Chern-Simons theory for the gapped bulk [77], and helical Luttinger liquid theory for the gapless edges [78, 79]. The above-mentioned requirement of at least four orbitals per unit cell (here the term orbital may also refer to spin or pseudospin) or, equivalently, four states at a given momentum \mathbf{k} in the noninteracting Bloch picture,

can be understood as follows: the two spin directions are related by time-reversal symmetry and hence degenerate. A band insulator, with a gap between filled valence bands and empty conduction bands and hence not adiabatically connected to the vacuum, then requires two sets of Kramers degenerate bands, and hence four bands in total [80].

While some features are generic for quantum spin Hall models, there are also model-specific aspects related to, for example, the crystal lattice. An important example is the potential quantum spin liquid phase of the KMH model, which was first reported for the Hubbard model on the honeycomb lattice [81]. This lattice has the smallest possible coordination number $z = 3$ in two dimensions, rendering quantum fluctuations particularly important. The honeycomb lattice is also at the centre of attention in condensed matter physics because of tremendous progress in preparing single layers or bilayers of graphene [82, 83].

Much of the work reviewed here uses the paradigmatic framework of a local Hubbard interaction to study electronic correlation effects [84]. This choice, usually motivated by simplicity, is assumed to capture the dominant physics. Models with nonlocal interactions play a key role for topological Mott insulators with dynamically generated spin-orbit interactions (see section 4.4), and for spinless models of Chern insulators (see section 4.5). Nonlocal interactions may also give rise to interesting new physics in helical liquids [79].

2.1. Kane-Mele-Hubbard model

The KM Hamiltonian was originally derived as a model for graphene, and can be written in the form [11, 12]

$$H_{\text{KM}} = -t \sum_{\langle i,j \rangle} \hat{c}_i^\dagger \hat{c}_j + i \lambda_{\text{SO}} \sum_{\langle\langle i,j \rangle\rangle} \hat{c}_i^\dagger (\boldsymbol{\nu}_{ij} \cdot \boldsymbol{\sigma}) \hat{c}_j \quad (1)$$

$$+ i \lambda_{\text{R}} \sum_{\langle i,j \rangle} \hat{c}_i^\dagger (\mathbf{s} \times \hat{\mathbf{d}}_{ij})_z \hat{c}_j.$$

Here $\hat{c}_i^\dagger = (c_{i\uparrow}^\dagger, c_{i\downarrow}^\dagger)$ is a spinor, and $c_{i\sigma}^\dagger$ creates an electron in a Wannier state at site i with spin σ . Pairs of nearest-neighbour and next-nearest-neighbour lattice sites are indicated by the symbols $\langle i, j \rangle$ and $\langle\langle i, j \rangle\rangle$, which also implicitly include the Hermitian conjugate terms.

The KM model (1) is defined on the honeycomb lattice spanned by the lattice vectors $\mathbf{a}_1, \mathbf{a}_2$, as shown in figure 1(a) (see caption for details). Nearest-neighbour sites are connected by the vectors $\pm \boldsymbol{\delta}_i$, $i = 1, 2, 3$. The honeycomb lattice has two lattice sites per unit cell, and together with the spin degree of freedom, there are four orbitals per unit cell. The Brillouin zone, shown in figure 1(b), contains the Dirac points K and K'.

The first term in (1) is the usual tight-binding hopping term between sites on different sublattices, which leads to the celebrated graphene band dispersion (here the lattice constant $a = 1$) [85]

$$\epsilon(\mathbf{k}) = \pm |g_{\mathbf{k}}| \quad (2)$$

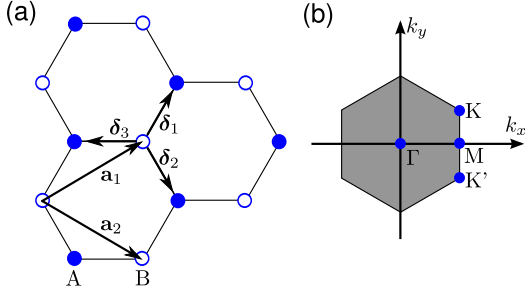


Figure 1. (a) The honeycomb lattice with lattice constant a consists of two sublattices A, B and is spanned by the basis vectors $\mathbf{a}_1 = \frac{1}{2}a(3, \sqrt{3})$, $\mathbf{a}_2 = \frac{1}{2}a(3, -\sqrt{3})$ (in the conventions of [83]). Nearest-neighbour lattice sites are connected by the vectors $\delta_1 = \frac{1}{2}a(1, \sqrt{3})$, $\delta_2 = \frac{1}{2}a(1, -\sqrt{3})$, and $\delta_3 = a(-1, 0)$. The hexagonal first Brillouin zone contains the two nonequivalent Dirac points $K = \left(\frac{2\pi}{3a}, \frac{2\pi}{3\sqrt{3}a}\right)$ and $K' = \left(\frac{2\pi}{3a}, -\frac{2\pi}{3\sqrt{3}a}\right)$.

$$= \pm t \left[3 + 2 \cos(\sqrt{3}k_y) + 4 \cos(3k_x/2) \cos(\sqrt{3}k_y/2) \right]^{1/2},$$

with Dirac cones at K and K'.

The spin-orbit interaction ($\sim \lambda_{\text{SO}}$) is described by a complex-valued next-nearest-neighbour hopping term with a sign ± 1 depending on the sublattice, the direction of the hop (i.e., left turn or right turn), and the spin orientation, as illustrated for a single hexagon in figure 2. This sign is encoded in $(\boldsymbol{\nu}_{ij} \cdot \boldsymbol{\sigma})$, where

$$\boldsymbol{\nu}_{ij} = \frac{\mathbf{d}_{ik} \times \mathbf{d}_{kj}}{|\mathbf{d}_{ik} \times \mathbf{d}_{kj}|}, \quad (3)$$

\mathbf{d}_{ik} is the three-dimensional vector (with vanishing z component) connecting sites i and k , and k is the intermediate lattice site involved in the hopping process from site i to site j . The vector $\boldsymbol{\sigma}$ is defined by the Pauli matrices as $\boldsymbol{\sigma} = (\sigma^x, \sigma^y, \sigma^z)$. Close to the Dirac points, the spin-orbit term can be written as $H_{\text{SO}} \sim \lambda_{\text{SO}} \psi^\dagger \sigma^z \tau^z s^z \psi$, where the Pauli matrices refer to the spin, sublattice, and Dirac point, respectively [12].

The last term in (1) is the Rashba spin-orbit interaction of strength λ_{R} , defined in terms of the spin vector $\mathbf{s} = \frac{1}{2}\boldsymbol{\sigma}$, and the unit vector $\hat{\mathbf{d}}_{ij} = \mathbf{d}_{ij}/|\mathbf{d}_{ij}|$. The Rashba coupling, which is purely off-diagonal in spin (hence, spin is no longer conserved), breaks the $z \mapsto -z$ inversion symmetry, and arises for example, in the presence of a substrate [12].

For $\lambda_{\text{SO}} \neq 0$, the KM model with zero chemical potential describes a quantum spin Hall insulator as long as $\lambda_{\text{R}} < 2\sqrt{3}\lambda_{\text{SO}}$ [11, 86], see also section 3. On a geometry with open edges, the KM model exhibits helical edge states with a symmetry-protected crossing at $k = 0$ ($k = \pi$) for armchair (zigzag) edges.

The KM-Hubbard (KMH) model corresponds to H_{KM} with an additional, local Hubbard repulsion between

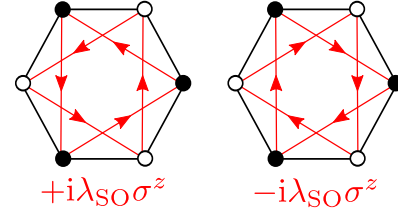


Figure 2. Sign structure of the spin-orbit term in the Kane-Mele model (1).

electrons, and is written as

$$H_{\text{KMH}} = H_{\text{KM}} + \frac{1}{2}U \sum_i (\hat{c}_i^\dagger \hat{c}_i - 1)^2. \quad (4)$$

It was first considered by Rachel and Le Hur [87]. Compared to the Hubbard model ($\lambda_{\text{SO}} = 0$), the spin-orbit terms reduce the rotational symmetry from the hexagonal point group C_6 to C_3 , and the spin rotation symmetry from $SU(2)$ to either $U(1)$ (for $\lambda_{\text{R}} = 0$) or Z_2 (for $\lambda_{\text{R}} \neq 0$). A detailed review of previous work on the KMH model is provided in sections 4 and 5, and the noninteracting case is considered in section 3.

The KMH model has played an important role because it can be investigated with exact quantum Monte Carlo methods. Moreover, there is a close connection to the Hubbard model on the honeycomb lattice, which after reports of the existence of an intermediate spin liquid phase [81] has been at the focus of intense investigations. The existence of a Mott metal-insulator transition at a finite critical U_c on the honeycomb lattice is a result of the vanishing density of states at the Fermi level, $N(\omega) \sim |\omega|$ [83], which renders the logarithmic instability toward magnetic order ineffective. This stability with respect to perturbations is a general property of Dirac points. In contrast, symmetry breaking and topological phases can arise for arbitrarily small interactions in models with quadratic band crossing points [88].

2.2. Haldane-Hubbard model

Although it breaks time-reversal symmetry and hence does not describe a quantum spin Hall state, the Haldane-Hubbard model (the name is somewhat misleading, because the interaction is nonlocal) is included here for two reasons. First, the noninteracting version [89] has played a key role for the development of the field of quantum spin Hall insulators as it underlies the KM model [11, 12]. Second, the interacting model has been studied in the context of topological quantum phase transitions [90–92].

The Hamiltonian can be written as

$$H_{\text{HH}} = -t_1 \sum_{\langle ij \rangle} c_i^\dagger c_j - t_2 \sum_{\langle\langle ij \rangle\rangle} e^{i\phi_{ij}} c_i^\dagger c_j + V \sum_{\langle ij \rangle} \hat{n}_i \hat{n}_j. \quad (5)$$

The first term describes the nearest-neighbour hopping of *spinless* fermions on the honeycomb lattice. The second

term is a spin-orbit coupling with a phase $\phi_{ij} = \pm\phi$ for clockwise (anticlockwise) next-nearest-neighbour hopping, equivalent to the spin-orbit term of the KM model (1) for a fixed spin direction. Also included is a repulsion V between spinless fermions at neighbouring lattice sites. Because of the restriction to spinless fermions (or, equivalently, to one spin sector), the Hamiltonian (5) breaks time-reversal symmetry, and for $V = 0$ realizes the *integer* quantum anomalous Hall effect at half filling [89]. Large enough interactions cause a quantum phase transition [90–92] to a charge-density-wave state, see section 4.

2.3. Bernevig-Hughes-Zhang-Hubbard model

The low-energy, continuum model for HgTe quantum wells involves two s and two p orbitals, each forming a Kramers pair, with a gap at the Γ point [23]. From this model, Bernevig *et al* [23] derived a two-dimensional tight-binding model on the square lattice. A possible real-space representation, hereafter referred to as the BHZ model, is [8]

$$H_{\text{BHZ}} = \sum_{\mathbf{i}} \sum_{\alpha} \sum_{\sigma} \epsilon_{\alpha} c_{\mathbf{i},\alpha,\sigma}^{\dagger} c_{\mathbf{i},\alpha,\sigma} - \sum_{\mathbf{i},\delta} \sum_{\alpha\beta} \sum_{\sigma} c_{\mathbf{i}+\delta,\alpha,\sigma}^{\dagger} [t_{\delta}^{\sigma}]^{\alpha\beta} c_{\mathbf{i},\beta,\sigma}, \quad (6)$$

where a labels the four bonds to nearest-neighbour lattice sites, $\alpha, \beta \in \{s, p\}$ are orbital indices, and σ is a spin index. The 2×2 hopping matrix defined in orbital space is given by (here $\text{sgn}(\sigma) = +1, -1$ for $\sigma = \uparrow, \downarrow$)

$$t_{\pm x}^{\sigma} = \begin{pmatrix} t_{ss} & \pm t_{sp} \\ \mp t_{sp} & -t_{pp} \end{pmatrix}, \quad (7)$$

$$t_{\pm y}^{\sigma} = \begin{pmatrix} t_{ss} & \pm i \text{sgn}(\sigma) t_{sp} \\ \pm i \text{sgn}(\sigma) t_{sp} & -t_{pp} \end{pmatrix}.$$

The momentum-space representation of the tight-binding model reduces to the continuum model for HgTe upon expanding around the Γ point [23]. A convenient choice of parameters is to set $\epsilon_s = -\epsilon_p \equiv \epsilon/2$, so that ϵ is the energy splitting between s and p orbitals, and $t_{ss} = t_{pp} \equiv t$. The energy bands are then given by

$$E(\mathbf{k}) = \pm 2 \left\{ 4t_{sp}^2 (\sin^2 k_x + \sin^2 k_y) + [\epsilon/2 - 2t(\cos k_x + \cos k_y)]^2 \right\}^{1/2}. \quad (8)$$

Writing the BHZ model in terms of Dirac matrices [8] and considering the eigenvalues of the parity operator at the time-reversal invariant points of the Brillouin zone gives a quantum spin Hall phase for $-8t < \epsilon < 8t$, and a trivial insulator else. This condition, when translated into the corresponding notations, agrees with previous work [8, 23, 93, 94]. However, as pointed out in [93], there are in fact two different topological phases, separated by a metallic point at $\epsilon = 0$. These phases have topological band gaps at the Γ point, $\Delta(\Gamma) = 4|\epsilon/2 - 4t|$, and at the M points,

$\Delta(M) = 2|\epsilon|$, respectively. They can be distinguished by their response to topological defects in the form of dislocations [93]. For systems with edges, the protected crossing point of the helical edge states is located at $k = 0$ (Γ phase) and $k = \pi$ (M phase), respectively. Only the Γ phase is observable in HgTe quantum wells [23], whereas the M phase is a feature of the tight-binding model.

The Hamiltonian (6) neglects terms that couple the two spin sectors which arise from the breaking of inversion and/or axial symmetry in HgTe quantum wells, but are expected to be small [23]. Nevertheless, the spin-conserved case is not generic. The effects of nonconserving terms have been discussed, for example, in [95, 96].

Because there are two orbitals per site, the definition of a local Hubbard interaction term is not unique, and both intra-orbital interactions of the form $H_U = U \sum_{i\alpha} \hat{n}_{i\alpha\uparrow} \hat{n}_{i\alpha\downarrow}$ [97–99] as well as intra- and interorbital interactions, $H_U = U \sum_i \hat{n}_i (\hat{n}_i - 1)$ (with $\hat{n}_i = \sum_{\alpha\sigma} \hat{n}_{i\alpha\sigma}$) [94] have been studied. For realistic calculations, the full Coulomb interaction (including Hund's rule coupling) should be taken into account [100]. Interaction effects on the edge states of the *BHZ-Hubbard* (*BHZH*) model have been explored in [96, 98, 99], whereas bulk properties were investigated in [94, 97, 98, 100, 101].

2.4. Sodium iridate model

Shitade *et al* [28] predicted a quantum spin Hall phase with substantial spin-orbit and electron-electron interactions in the transition-metal oxide Na_2IrO_3 . Exploiting the layered structure of this material, they derived an effective, two-dimensional model on the honeycomb lattice. The Hamiltonian takes the form [28, 31, 102]

$$H_{\text{SI}} = -t \sum_{\langle ij \rangle} \sum_{\sigma} c_{i\sigma}^{\dagger} c_{j\sigma} + \sum_{\langle\langle ij \rangle\rangle} \sum_{ss'} c_{is}^{\dagger} [t_{ij}]^{ss'} c_{js'} + U \sum_i \hat{n}_{i\uparrow} \hat{n}_{i\downarrow}. \quad (9)$$

It describes nearest-neighbour and next-nearest-neighbour electron hopping between Ir atoms. The indices s, s' refer to pseudospin states [28], but will also be called spin states in the following. The nearest-neighbour hopping (t) is real and diagonal in spin. The next-nearest-neighbour hopping in general has real and complex contributions [28],

$$[t_{ij}]^{ss'} = -t_1 \delta_{ss'} + it_2 \sigma_{ss'}^w, \quad (10)$$

where $w = x, y, z$ selects one of the Pauli matrices depending on the hopping path, as illustrated in figure 3. The contribution t_1 is sometimes neglected.

In contrast to the KM model (1), there is only one parameter t_2 that determines the strength of both spin-conserving and nonconserving hopping processes. Spin is therefore generically not conserved in the SI model. Moreover, both contributions act between next-nearest-neighbour lattice sites, whereas the spin-orbit and Rashba terms in the KM model (1) connect next-nearest and

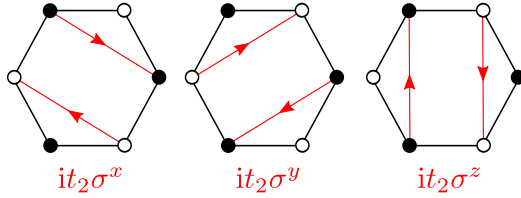


Figure 3. Spin-orbit terms of the SI model (9), see also [28].

nearest-neighbour sites, respectively. The helical edge states cross at $k = 0$ ($k = \pi$) on armchair (zigzag) edges.

The model (9) describes a single honeycomb layer of Ir atoms in Na_2IrO_3 , and may be realized at the surface of a three-dimensional sample [28]. In contrast to the KMH model for graphene and the BHZH model for HgTe, strong electron-electron interactions have been argued to be generically present in Na_2IrO_3 [28]. The SI model has been studied in [31, 32, 102].

2.5. Other models

Whereas a minimum of four states per unit cell is necessary for a gapped, time-reversal invariant band structure, there exist several examples of more complex models that support a quantum spin Hall state. These include the kagomé lattice [103], the decorated honeycomb lattice [104], the Lieb lattice [105], the square-octagon lattice [106], and the ruby lattice [107]. The corresponding multi-band Hamiltonians are of particular interest for two reasons. First, the decorated honeycomb lattice has been shown to provide a remarkable connection between a noninteracting topological state (the quantum spin Hall state) and a strongly interacting topological state (the chiral spin liquid phase of the Kitaev model [108, 109]), both of which are exactly solvable [76, 104]. Second, such models can have band structures that include very flat bands, and thereby possess the potential for fractional topological states arising from electrons in strongly correlated, partially filled flat bands [107], see also section 4.5. Finally, whereas a quantum spin Hall state on the honeycomb lattice requires complex next-nearest-neighbour hopping, *nearest-neighbour* hopping is sufficient on more complicated lattices such as the kagomé or the decorated honeycomb lattices [104].

Other models that are relevant in the context of correlation effects were proposed by Araújo *et al* [110] (a bilayer square-lattice model), Goryo and Maeda [111] (the bilayer KMH model), and Cocks *et al* [112] (a time-reversal invariant version of the Hofstadter problem). Finally, lattice models for topological Mott insulators and fractional topological insulators will be discussed in sections 4.4 and 4.5, respectively.

3. Noninteracting quantum spin Hall insulator

Although this review is mainly concerned with correlation effects, a brief summary of the noninteracting case provides the starting point for the discussion of interacting systems. It also illustrates the key concepts of time-reversal invariance, the bulk-boundary correspondence, and topological protection. For concreteness, the example of the KM model (1) is used. More general reviews have been given in [14, 50].

The KM model (1) can be solved exactly by Fourier transformation. In the absence of a Rashba term, it can be written in the form $H_{\text{KM}} = \sum_{\mathbf{k}} \Psi_{\mathbf{k}}^{\dagger} H(\mathbf{k}) \Psi_{\mathbf{k}}$, with

$$H(\mathbf{k}) = \begin{pmatrix} \gamma_{\mathbf{k}} & -g_{\mathbf{k}} & 0 & 0 \\ -g_{\mathbf{k}}^* & -\gamma_{\mathbf{k}} & 0 & 0 \\ 0 & 0 & -\gamma_{\mathbf{k}} & -g_{\mathbf{k}} \\ 0 & 0 & -g_{\mathbf{k}}^* & \gamma_{\mathbf{k}} \end{pmatrix} = \begin{pmatrix} H^{\dagger}(\mathbf{k}) & 0_{2 \times 2} \\ 0_{2 \times 2} & H^{\downarrow}(\mathbf{k}) \end{pmatrix} \quad (11)$$

and $\Psi_{\mathbf{k}}^{\dagger} = (a_{\mathbf{k}\uparrow}^{\dagger}, b_{\mathbf{k}\uparrow}^{\dagger}, a_{\mathbf{k}\downarrow}^{\dagger}, b_{\mathbf{k}\downarrow}^{\dagger})$. Here a and b operators refer to the two sublattices of the honeycomb lattice, see figure 1; $g_{\mathbf{k}} = t \sum_i e^{i\mathbf{k} \cdot \delta_i}$ is related to the nearest-neighbour hopping (see (2)), whereas the spin-orbit coupling enters via $\gamma_{\mathbf{k}} = 2\lambda_{\text{SO}} [2 \cos(3k_x/2) \sin(\sqrt{3}k_y/2) - \sin(\sqrt{3}k_y)]$. From (11) it is quite obvious that the KM model can be regarded as two decoupled models for the \uparrow and \downarrow spins, each equivalent to the spinless Haldane model (5), and described by the 2×2 matrices $H^{\sigma}(\mathbf{k})$. The two spin sectors become coupled in the presence of Rashba terms, see (1).

Because time-reversal symmetry is inherently linked to the quantum spin Hall insulator, it is worth considering the corresponding transformation of (11). For spin-1/2 fermions, the time-reversal operator can be written as $\hat{\Theta} = \exp(i\pi\sigma^y)\hat{K}$ [8, 50], where σ^y is a Pauli matrix and \hat{K} denotes complex conjugation. Application of $\hat{\Theta}$ to a single-particle Bloch state leads to $\mathbf{k} \mapsto -\mathbf{k}$ and flipping of the spin. Interchanging the \uparrow and \downarrow sectors of (11), taking the complex conjugate, and using $\gamma_{-\mathbf{k}} = -\gamma_{\mathbf{k}}$ and $g_{-\mathbf{k}} = g_{\mathbf{k}}^*$, one can verify that the KM Hamiltonian indeed has the symmetry $H(-\mathbf{k}) = \hat{\Theta}H(\mathbf{k})\hat{\Theta}^{-1}$. In contrast, this is not the case for the spinless Haldane model [9] (equation (5)).

The eigenvalues of (11) are

$$E^{\pm}(\mathbf{k}) = \pm \sqrt{|g_{\mathbf{k}}|^2 + \gamma_{\mathbf{k}}^2}, \quad (12)$$

so that the spectrum has two bands, each of which has a Kramers degeneracy between $\sigma = \uparrow$ and $\sigma = \downarrow$. For $\lambda_{\text{SO}} = 0$, the band structure reduces to (2), and the familiar gapless Dirac spectrum is recovered at the points K, K'. Equation (12) shows that any nonzero spin-orbit coupling λ_{SO} opens a gap $\Delta_{\text{SO}} = 3\sqrt{3}\lambda_{\text{SO}}$ at the Dirac points [12, 87]. For $\lambda_{\text{SO}}/t > 1/(3\sqrt{3}) \sim 0.2$, the minimal gap of size $\Delta = 2t$ is instead found at the M points [87].

In the Haldane model, the spin-orbit term gives rise to an integer Chern invariant, a chiral edge mode,

and a Hall conductivity $\sigma_{xy} = \pm e^2/h$ [9]. The key observation of Kane and Mele [11, 12] was that combining two copies of the Haldane model, with Hall conductivities $\sigma_{xy}^\uparrow = -\sigma_{xy}^\downarrow$ (the opposite sign is apparent from the diagonal matrix elements in (11)), leads to a model of spinful fermions that preserves time-reversal symmetry. Remarkably, this construction—dubbed the *Haldane-Kane-Mele correspondence* in [76]—extends to interacting systems with and without intrinsic spin-orbit coupling, and even to fractional states [41]. Whereas the Hall conductivity $\sigma_{xy} = \sigma_{xy}^\uparrow + \sigma_{xy}^\downarrow = 0$, as required by the fact that σ_{xy} is odd under time reversal, the spin Hall conductivity $\sigma_{xy}^s = (\hbar/2e)(\sigma_{xy}^\uparrow - \sigma_{xy}^\downarrow)$, related to the spin current $\mathbf{J}_s = (\hbar/2e)(\mathbf{J}_\uparrow - \mathbf{J}_\downarrow)$, takes on nonzero values $\sigma_{xy}^s = \pm e/2\pi$ [12]. The sign of σ_{xy}^s depends on the sign of the spin-orbit coupling λ_{SO} [86]. The quantization of σ_{xy}^s holds as long as spin is conserved, but a nonzero spin Hall conductivity exists under more general conditions [12].

Remarkably, the quantum spin Hall phase of the KM model, which does not break any symmetries, represents a new state of matter that is topologically distinct from a simple band insulator [11, 12]. This distinction and the topological character of the quantum spin Hall state are a consequence of time-reversal symmetry, which gives rise to a symmetry-protected topological state [45], see section 1.

In close analogy to the integer quantum Hall effect [4, 113], a topological invariant can be defined. An explicit mathematical definition is most easily achieved when spin is conserved and the quantum spin Hall state decouples into two integer quantum Hall states, as described by (11). For a noninteracting, integer quantum Hall system, the Chern invariant for the m -th band is given by [4–6, 114]

$$C_m = \frac{1}{2\pi} \int d^2\mathbf{k} \mathcal{F}_m(\mathbf{k}), \quad (13)$$

where $\mathcal{F}_m(\mathbf{k}) = \nabla_{\mathbf{k}} \times \mathcal{A}_m(\mathbf{k})$ is the so-called *Berry flux* or *Berry curvature* (a gauge-invariant, local quantity), and $\mathcal{A}_m = i \langle u_m | \nabla_{\mathbf{k}} | u_m \rangle$ is the *Berry phase* or *Berry connection* (whose line-integral around a closed loop in momentum space gives the phase picked up by the Bloch state $|u_m\rangle$) [114]. A particularly simple representation can be obtained for a 2×2 Hamiltonian, such as $H^\sigma(\mathbf{k})$ in (11). Writing the Hamiltonian as $H^\sigma(\mathbf{k}) = \mathbf{h}^\sigma(\mathbf{k}) \cdot \boldsymbol{\sigma}$, and defining the unit vector field $\hat{\mathbf{h}}^\sigma(\mathbf{k}) = \mathbf{h}^\sigma(\mathbf{k})/|\mathbf{h}^\sigma(\mathbf{k})|$, the Chern number reads [115, 116]

$$C^\sigma = \frac{1}{4\pi} \int d^2\mathbf{k} \left[\partial_{k_x} \hat{\mathbf{h}}^\sigma(\mathbf{k}) \times \partial_{k_y} \hat{\mathbf{h}}^\sigma(\mathbf{k}) \right] \cdot \hat{\mathbf{h}}^\sigma(\mathbf{k}). \quad (14)$$

In this case, the topological invariant corresponds to the winding number of the mapping $\hat{\mathbf{h}}^\sigma(\mathbf{k})$ between the Brillouin zone and the unit sphere; mathematically, nonzero values of C^σ require three nonzero components of the vector $\hat{\mathbf{h}}^\sigma(\mathbf{k})$, which physically corresponds to broken time-reversal symmetry [116].

For a quantum spin Hall insulator with time-reversal symmetry, as described by (11) for $\lambda_{\text{SO}} \neq 0$, the Chern

indices have opposite sign, so that $C^\uparrow + C^\downarrow = 0$. However, the *spin Chern number* [86, 117] $C^s = (C^\uparrow - C^\downarrow)/2 = \pm 1$ is nonzero, and the Z_2 topological invariant defined by [50]

$$\nu = C^s \bmod 2 \quad (15)$$

takes on the values 0, 1. If spin is conserved ($\lambda_{\text{R}} = 0$), ν is directly related to the quantized spin Hall conductivity, $\sigma_{xy}^s = \pm \nu e/2\pi$. Hence $\nu = 1$ corresponds to the topologically nontrivial state that exhibits the quantum spin Hall effect. When spin is not conserved, it is no longer possible to calculate ν from the Chern indices C^\uparrow and C^\downarrow , and σ_{xy}^s is no longer quantized to $\pm e/2\pi$. Nevertheless, a quantum spin Hall phase with quantized $\nu = 1$ persists [11, 86]. The calculation of the topological invariant of systems without spin conservation, and with interactions and/or disorder will be the topic of section 6.

The existence of a topological state in the KM model relies on the special form of the spin-orbit term. The topological band structure arises from the opposite sign of the spin-orbit gap at K and K' in the presence of inversion symmetry. Explicitly, $\gamma_{\text{K}'} = -\gamma_{\text{K}}$, as can be verified using the definition of γ given after (11) and the definition of the Dirac points in figure 1. As a counter example, a gap in the spectrum can also be opened by adding a staggered sublattice potential, $\lambda_v \sum_i \xi_i \hat{c}_i^\dagger \hat{c}_i$, with $\xi_i = \pm 1$ depending on the sublattice. Such a term, which preserves time-reversal symmetry but breaks inversion symmetry [9, 118], has the same sign at K and K' , and leads to a topologically trivial insulator with $\nu = 0$ [9, 11, 12]. It is expected to be generically present in silicene as a result of buckling [16]. The topological phase can be destroyed when the gap is closed by competing terms such as Rashba spin-orbit coupling [11, 86].

Similar to the quantum Hall effect, the fact that the quantum spin Hall phase is topologically distinct from a simple band insulator has important consequences. As implied by the term topological, such a state cannot be connected to a nontopological state via adiabatic transformations of the Hamiltonian. Instead, a transition from a quantum spin Hall state to a topologically trivial state can occur either via a closing of the bulk band gap, or via the breaking of time-reversal symmetry [45].

Because a closing of the gap is required in a system with time-reversal symmetry, an interface between a quantum spin Hall insulator and a trivial insulator such as the vacuum necessarily gives rise to metallic states [50]. The existence of these states may also be inferred from a flux insertion argument [119]. Whereas all electrons at a given edge of a quantum Hall sample move in the same direction (*chiral edge state*) [120], quantum spin Hall insulators have *helical edge states* [78]: at each edge, electrons with spin \uparrow move in one direction and electrons with spin \downarrow move in the opposite direction. Hence, there is a one-to-one correspondence between spin and direction of motion in helical edge states [12, 78]. The existence of pairs of edge states with opposite chirality follows directly from

equation (11), which combines two independent integer quantum Hall states that possess chiral edge modes of opposite velocity.

For noninteracting systems, the number of pairs of edge states (modulo 2) is directly linked to the value of the Z_2 topological invariant ν [11, 50]. Moreover, the so-called *bulk-boundary correspondence* expresses the fact that the existence of edge states is guaranteed by the topological nature of the bulk system. This correspondence goes back to the work of Halperin [7]. It also follows from topological field theory when imposing gauge invariance [121], see below. Intuitively, it can be understood as a consequence of the protection of the topological state with respect to adiabatic deformations, implying that the only way to achieve a change of the topological invariant is by closing the bulk band gap. Such a closing, which can either occur as a function of a parameter (phase transition), or at the interface with another material (including the vacuum), is tantamount to the existence of gapless excitations. Hence, edge properties can in principle be studied to infer the properties of the bulk, but as discussed in sections 5 and 6, this equivalence can break down in interacting systems. For the latter, important progress has been made using the concept of symmetry-protected topological states [44–49].

As long as time-reversal symmetry is preserved, the quantum spin Hall state cannot be destroyed by small perturbations such as disorder or electron-electron interactions [11, 12, 78, 79]. Exploiting the bulk-boundary correspondence, this stability can be understood by considering the helical edge states. Denoting the band dispersion of the edge states by $\epsilon_\sigma(k)$ (where k is the conserved component of the two-dimensional crystal momentum along the edge) time-reversal symmetry leads to the condition

$$\epsilon_\downarrow(-k) = \epsilon_\uparrow(k). \quad (16)$$

At the special, time-reversal invariant momenta $k = 0, \pi$ (these points are mapped onto themselves under the action of $\hat{\Theta}$), this condition implies

$$\epsilon_\uparrow(k) = \epsilon_\downarrow(k), \quad k = 0, \pi, \quad (17)$$

and hence a symmetry-protected, gapless crossing point of edge states. It turns out that in the topological phase of the KM model, there exists a single pair of edge states that cross either at $k = 0$ for an armchair edge, or at $k = \pi$ for a zigzag edge [11, 12]. The latter case is illustrated in figure 4(a) for a ribbon with open boundaries in the y direction, whereas the armchair case can be seen in figure 16. The existence of only one crossing illustrates the fact that these states are edge states, and hence do not cover the entire Brillouin zone. The edge states in figure 4(a) connect the Dirac points K and K' , and their helicity becomes apparent by plotting the spin-resolved single-particle spectrum.

Because time-reversal symmetry implies degenerate edge states at either at $k = 0$ or $k = \pi$ [12], perturbations

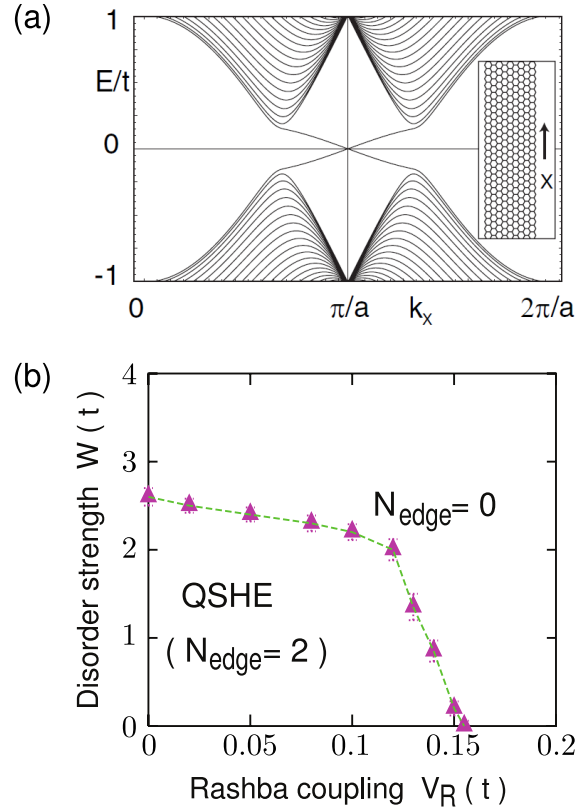


Figure 4. (a) Edge states of the KM model on a zigzag ribbon with open boundary conditions in the y direction (see inset) and $\lambda_{\text{SO}}/t = 0.03$ [12]. (Reprinted with permission from [12]. Copyright 2005 by the American Physical Society). (b) Phase diagram of the KM model as a function of Rashba coupling V_R and disorder strength W , at fixed spin-orbit coupling $V_{\text{SO}}/t = 0.05$ [86]. (Adapted with permission from [86]. Copyright 2006 by the American Physical Society).

that preserve time-reversal symmetry cannot open a gap. Most importantly, single-particle backscattering, which is the most relevant perturbation in ordinary one-dimensional metals [122], is not allowed in a helical liquid because the single-particle states $|k, \uparrow\rangle$ and $|-k, \downarrow\rangle$ are Kramers partners, and therefore orthogonal. Consequently, helical edge states are symmetry-protected from elastic, single-particle backscattering [12, 14, 78, 79], but the protection is weaker than that of chiral edge states in a quantum Hall insulator where all electrons at a given edge propagate in the same direction, and there is no phase space for backscattering. The presence of counter-propagating electrons at a given edge has important implications for strongly interacting systems, see section 5. Finally, single-particle backscattering is not forbidden by symmetry if an even number of edge states exists for each spin direction. This case corresponds to a trivial phase ($\nu = 0$) [78, 79].

The stability of the edge states with respect to disorder and Rashba spin-orbit coupling has been numerically verified [11, 86, 123], and the resulting phase diagram is reproduced in figure 4(b). The topological phase exists as long as the Rashba coupling does not exceed the value

$\lambda_R = 2\sqrt{3}\lambda_{SO}$ [12] (note that the coupling constant λ_{SO} used here and V_{SO} used in [86] differ by a prefactor), and up to a critical value of the disorder strength. This result is crucial for the experimental realization of the quantum spin Hall effect [20, 21] because neither Rashba coupling nor disorder can be completely excluded. In the presence of interactions, the stability of the edge states is no longer guaranteed, as discussed in section 5.

As shown in this section, many aspects of integer quantum Hall and spin Hall insulators can be understood in the framework of topological band theory [14]. However, the latter is inherently restricted to noninteracting systems. An alternative approach to topological states of matter is based on Chern-Simons field theory, a low-energy theory of gauge fields that is applicable to interacting and even fractional states. A comprehensive introduction to Chern-Simons theory can be found, for example, in [3]. For the extension to topological insulators with time-reversal symmetry see [77].

To illustrate how Abelian Chern-Simons theory explains the quantization of σ_{xy} as well as the presence of edge states in a quantum Hall insulator, it is sufficient to consider the noninteracting Haldane model in the form $H = \sum_{ij} t_{ij} c_i^\dagger c_j$, cf. (5), minimally coupled to an electromagnetic field,

$$H(A^\mu) = \sum_{ij} t_{ij} c_i^\dagger c_j \exp \left[\frac{2\pi i}{\Phi_0} \int_i^j \mathbf{A}(\mathbf{l}, t) \cdot d\mathbf{l} \right] + ec \sum_i A_0(i, t) c_i^\dagger c_i. \quad (18)$$

The scalar and vector potentials may be combined in the form $A^\mu \equiv (A_0, -\mathbf{A})$ with $A_0 = \Phi/c$ and $\mathbf{A} = (A_1, A_2)$. Gauge invariance implies $\partial_\mu j^\mu = 0$ with $j^\mu = -\delta H / \delta A_\mu$. Linear response theory then directly gives the quantized Hall conductivity.

The starting point for the derivation of Chern-Simons theory is the Grassmann path integral [43]

$$Z(A_\mu) = \int \prod_i dc_i^\dagger dc_i e^{iS(A_\mu)} \quad (19)$$

with the action

$$S(A_\mu) = \int dt \left\{ \sum_i c_i^\dagger(t) \left[\delta_{ij} i\partial_t - t_{ij} \right] c_j(t) + \sum_i j^\mu(i, t) A_\mu(i, t) \right\}. \quad (20)$$

Equation (20) follows from a gradient expansion in A^μ . The fermions can be integrated out, at the expense of a Gaussian integral, to obtain $Z(A_\mu) = e^{iS_{\text{eff}}(A_\mu)}$ with

$$S_{\text{eff}}(A_\mu) = \int \int dt dt' \sum_{ij} A_\mu(i, t) \times P^{\mu\nu}(i, t, j, t') A_\nu(j, t'). \quad (21)$$

Here $P^{\mu\nu}$ is the current-current correlation function, which is short-ranged in an insulating state, and a summation over repeated Greek indices is implied. Hence, to a first approximation, retardation effects can be omitted by setting $t' = t$. Taking the continuum limit, all possible gauge invariant terms can be derived. The relevant contribution for topological states is the Chern-Simons term

$$S_{\text{eff}}^{\text{CS}}(A_\mu) = C \frac{e^2}{4\pi} \epsilon^{\mu\nu\rho} \int d^2x \int dt A_\mu \partial_\nu A_\rho \quad (22)$$

from which all the low-energy properties of the integer quantum Hall state follow. The invariance of the theory with respect to twists of the boundary conditions by a multiple of the flux quantum Φ_0 pins the first Chern number C to an integer [4, 5]. Using $j_\mu = \delta S_{\text{eff}}^{\text{CS}} / \delta A_\mu$, and assuming $A_0 = 0$, gives the familiar quantized Hall response

$$j_x = \sigma_{xy} E_y, \quad \sigma_{xy} = C \frac{e^2}{h}. \quad (23)$$

On a torus geometry, the Chern-Simons action (22) is invariant under the gauge transformation $A_\mu \rightarrow A_\mu + \partial_\mu \chi$. However, in the presence of a boundary (e.g., on a cylinder), the gauge transformation leads to an additional boundary term that is directly related to the chiral edge state of a quantum Hall insulator [3].

Finally, a Chern-Simons theory of a noninteracting, spin-conserving quantum spin Hall insulator (as appropriate for the KM model) takes the form

$$S_{\text{QSH}}^{\text{CS}} = \frac{e^2}{4\pi} \epsilon^{\mu\nu\rho} \int d^2x \int dt \left(A_\mu^\dagger \partial_\nu A_\rho^\dagger - A_\mu^\dagger \partial_\nu A_\rho^\dagger \right). \quad (24)$$

For more general cases, including fractional topological states, see [124] and references therein.

4. Bulk correlation effects

The integer quantum spin Hall effect can be understood purely in terms of the band structure. Much of the recent theoretical work has focused on the impact of electronic correlations. Given the scope of this review, the discussion of bulk correlation effects begins with results for models with intrinsic spin-orbit coupling that support an integer quantum spin Hall state in the noninteracting limit. The investigation of such systems is particularly rewarding as the corresponding models are amenable to numerical methods, including exact quantum Monte Carlo simulations that permit to investigate, for example, the critical behaviour at quantum phase transitions. After an overview of phenomena using the example of the intensely studied KMH model, a detailed discussion of correlated quantum spin Hall phases and interaction-driven phase transitions with or without symmetry breaking is given, followed by two shorter sections on interaction-driven topological insulators, and fractional topological insulators.

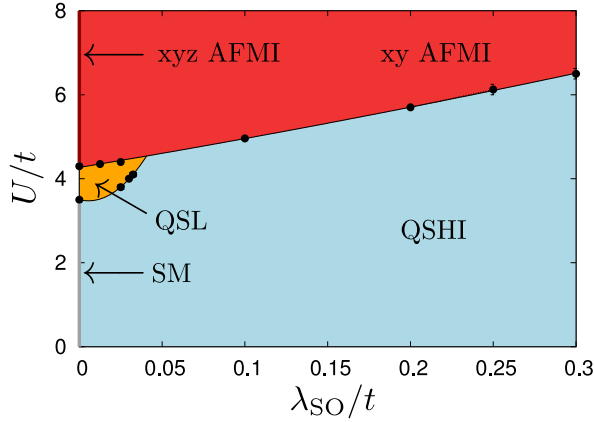


Figure 5. Phase diagram of the half-filled KMH model from quantum Monte Carlo simulations [125–127]. The phases correspond to a semimetal (SM, for $\lambda_{\text{SO}} = 0$), a quantum spin Hall insulator (QSHI), a quantum spin liquid (QSL), and an antiferromagnetic Mott insulator (AFMI) with either Heisenberg (for $\lambda_{\text{SO}} = 0$) or easy plane (for $\lambda_{\text{SO}} \neq 0$) order. Here $\lambda_{\text{R}} = 0$. Data taken from [125–127].

4.1. Phases of the Kane-Mele-Hubbard model

The KMH model provides a framework to study the effects of electronic correlations on a quantum spin Hall insulator. It is of particular interest because of connections with graphene [83] and the Hubbard model on the honeycomb lattice [81]. Given its historical importance and the possibility of applying exact quantum Monte Carlo methods, the KMH model is arguably the best understood model among those introduced in section 2.

Figure 5 shows the numerically obtained [125–127] phase diagram of the KMH model at half filling, and with conserved spin ($\lambda_{\text{R}} = 0$). Most importantly, the numerical results confirm the stability of the topological state of the KM model ($U = 0$) up to Hubbard interactions $U/t \gtrsim 4$, as first predicted based on mean-field theory [87]. As discussed in more detail below, the numerical results suggest that the topological phase at $U > 0$ is adiabatically connected to the noninteracting case. Even stronger electron-electron repulsion drives a quantum phase transition to a magnetic state discussed in detail in section 4.3. The other phases of the KMH model shown in figure 5 are a semimetal (SM) that exists for vanishing spin-orbit coupling (with a massless Dirac spectrum similar to (2)), and possibly a gapped quantum spin liquid (QSL) phase at intermediate U/t [81] to be discussed in section 4.3. Contrary to analytical predictions [128], numerical studies so far indicate that all phase transitions in figure 5 are continuous [126].

The phase diagram of the KMH model has been investigated by a variety of theoretical methods. Mean-field theory captures the magnetic transition, and the increase of the critical U with increasing λ_{SO} [87]. Quantum Monte Carlo simulations provide the exact phase boundary for the magnetic phase, demonstrate the absence of magnetic

order in the z direction, and suggest the existence of a quantum spin liquid phase [125, 126, 129]. (Figure 17 shows the numerical phase diagram obtained by Zheng *et al* [129].) Approximate variational Monte Carlo results are also available at $\lambda_{\text{SO}}/t = 0.1$ [130]. Quantum cluster methods such as the cluster dynamical mean-field theory [131] and the variational cluster approach [132, 133] are able to capture the overall structure of the phase diagram. However, care has to be taken regarding the choice of the cluster shape and size (a detailed discussion of the impact of nonlocal correlations in the Hubbard model on the honeycomb lattice can be found in [134]). Analytical approaches include slave-boson [135], slave-spin [136] and slave-rotor methods [94], as well as mappings to spin models to explore the regime of large U/t [31, 32, 137]. Using field theory and symmetry arguments, predictions about the phases and phase transitions of the KMH model were made by Griset and Xu [128] as well as by Lee [138].

With the exception of the quantum spin liquid phase, whose existence is still under debate [81, 125, 126, 139] and expected to be specific to the honeycomb lattice, the phase diagram in figure 5 contains many features that are generic for models of correlated quantum spin Hall insulators. In addition to the Z_2 topological phase, a semimetal also exists in the SI model (9) with $t_1 = t_2 = 0$ (where it reduces to the Hubbard model on the honeycomb lattice), and in the BHZH model at the metallic point $\epsilon = 0$. A quantum phase transition to a magnetic state with easy-plane order (as a result of spin-orbit coupling) at large U/t has also been observed in the BHZH model [94, 97], the SI model [102], and a spinful version of the Hofstadter butterfly problem with a Hubbard interaction [112]. The existence of a magnetic phase is a direct consequence of the nonfrustrated exchange interactions that emerge on bipartite lattices. Similarly, a correlation-driven transition from a topological to a magnetic state is also expected in three dimensions [36].

4.2. Correlated topological band insulators

In section 3, the bulk-boundary correspondence was invoked to argue that the quantum spin Hall phase should be stable as long as time-reversal symmetry is not broken. This idea is borne out by the phase diagram in figure 5, which shows that (with the possible exception of the region around the spin liquid phase) the topological state is eventually destroyed when time-reversal symmetry is spontaneously broken. However, throughout the quantum spin Hall phase, the bulk gap remains open upon switching on the Hubbard interaction, see Fig. 6. The topological character of this phase at $U > 0$ also manifests itself through its response to π fluxes [127], see section 6. These results firmly establish an adiabatic connection between the quantum spin Hall states with $U = 0$ and $U > 0$. Such behaviour seems to be typical of models that conserve spin [31]. On the other hand, an interaction-driven transition to a fractional

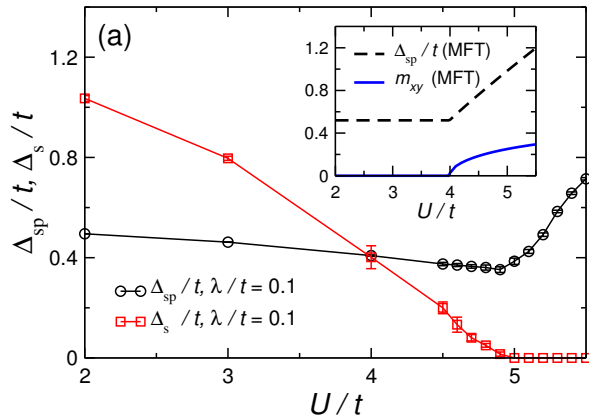


Figure 6. Single-particle gap Δ_{sp} and spin gap Δ_{s} of the KMH model as a function of U at $\lambda \equiv \lambda_{\text{SO}} = 0.1t$ [126]. At the transition ($U_c/t = 4.95(5)$), Δ_{sp} shows a dip, whereas Δ_{s} closes. Inset: Δ_{sp} and magnetization from mean-field theory. (Reprinted with permission from [126]. Copyright 2012 by the American Physical Society).

topological state that preserves time-reversal symmetry has been reported for the SI model [102] (see section 4.3).

Given a correlated quantum spin Hall insulator that exists up to rather large values of U/t , an important question is to what extent this phase resembles that of the noninteracting KM model (even if the phase is adiabatically connected to the noninteracting state, there could be substantial quantitative differences). A partial answer is provided by the quantum Monte Carlo results for the single-particle gap Δ_{sp} and the spin gap Δ_{s} shown in figure 7. Starting in the correlated semimetal phase at $U/t = 2$, any nonzero spin-orbit coupling λ_{SO} opens both gaps simultaneously. Importantly, for small λ_{SO} , both gaps follow very closely the corresponding results for the $U = 0$ KM model (indicated by the lines in figure 7), namely $\Delta_{\text{sp}} = \Delta_{\text{SO}} = 3\sqrt{3}\lambda$ and $\Delta_{\text{s}} = 2\Delta_{\text{sp}}$. This observation suggests that the quantum spin Hall states with $U/t = 2$ and $U/t = 0$ are very similar. Minor correlation effects are apparent from the fact that the gaps for $U/t = 2$ are systematically smaller than those for $U/t = 0$, and that $\Delta_{\text{s}} < 2\Delta_{\text{sp}}$.

Yoshida *et al* [97] have used dynamical mean-field theory to calculate the spin Hall conductivity of the BHZH model as a function of temperature and the intra-orbital repulsion U . The results, shown in figure 8, reveal a clear suppression of σ_{xy}^s due to thermal fluctuations and electronic correlations, and that σ_{xy}^s eventually vanishes at $U/t \sim 12$. However, as demonstrated in the inset, for small enough U/t , the conductivity extrapolates to the quantized value e^2/h for $T \rightarrow 0$. Consequently, although interaction effects are clearly visible at finite temperatures, the correlated quantum spin Hall phase of the BHZH model resembles the noninteracting state at $T = 0$. As pointed out in section 3, a nonquantized Hall conductivity is also observed in the noninteracting case when spin is not conserved; however, the topological invariant retains

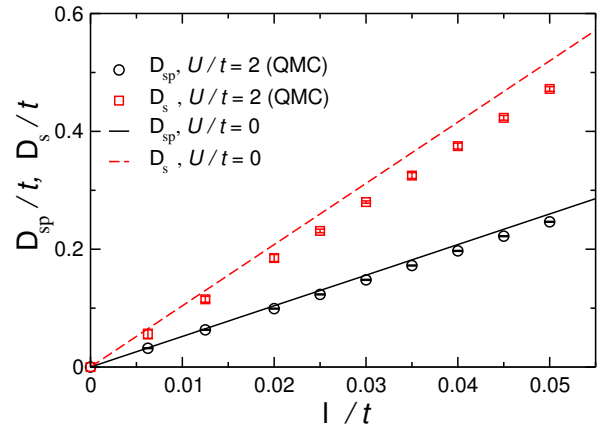


Figure 7. Single-particle gap Δ_{sp} and spin gap Δ_{s} as a function of spin-orbit coupling $\lambda \equiv \lambda_{\text{SO}}$ from quantum Monte Carlo simulations of the KMH model with $U/t = 2$ [126]. Also shown are the gaps of the noninteracting KM model (see text). (Reprinted with permission from [126]. Copyright 2012 by the American Physical Society).

its integer value $\nu = 1$ [86]. It would be interesting to confirm this explicitly in an interacting model, see also section 6. Temperature effects on the quantum spin Hall phase of the KMH model have been discussed in [131]. The topological nature of the quantum spin Hall phase at $U > 0$ has also been demonstrated for the KMH model both at $T = 0$ and $T > 0$ with the help of π fluxes [127]. Finally, the topological invariant of the KMH model has been calculated using the variational cluster approach [133].

The properties of the correlated quantum spin Hall phase have further been explored by numerically calculating the single-particle spectrum in systems with edges, see section 5. Both for the KMH model [131, 132] and the BHZH model [98], gapless helical edge states are observed even for substantial values of U/t , although interaction effects modify the spectral weight, edge transport and magnetic correlations (see section 5). In summary, in the spin-conserving KMH model, the quantum spin Hall phase remains qualitatively unaffected by correlations up to the point where it breaks down, in accordance with the expected adiabatic connection to the noninteracting spin Hall state. This finding has been exploited to construct an effective model of the edge states in which a Hubbard interaction is only taken into account at the edge, whereas the noninteracting bulk establishes the topological phase [125, 140].

4.3. Interaction-driven phase transitions

Although the quantum spin Hall phase of, for example, the KMH model persists even in the presence of rather strong interactions, it eventually breaks down at the onset of long-range magnetic order that spontaneously breaks both the $U(1)$ spin symmetry and time-reversal symmetry [87, 125, 129]. Such a magnetic transition is a generic feature of many quantum spin Hall models. In the KMH model, it can be studied in detail by quantum Monte Carlo

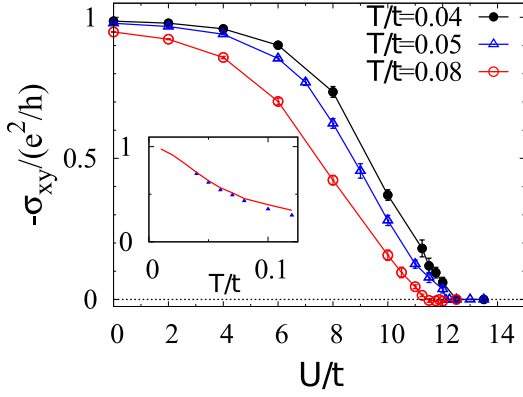


Figure 8. Spin Hall conductivity as a function of interaction strength and for different temperatures, as obtained from dynamical mean-field calculations for the BHZ model with intra-orbital repulsion U [97]. (Reprinted with permission from [97]. Copyright 2012 by the American Physical Society).

simulations. Whereas the magnetic transition involves a well-defined order parameter and can be captured already in mean-field theory, interactions can also lead to more complex phenomena in which quantum fluctuations play a key role. These include topological Mott insulators [35], quantum spin Hall states with Mott insulating edges [36, 87], or quantum spin liquids [125]. It is even possible to have a coexistence of a topological insulator with protected edge states and long-range magnetic order [141].

4.3.1. Symmetry-breaking transitions The best studied example of an interaction-driven quantum phase transition that involves the breaking of time-reversal symmetry is the magnetic transition observed in the KMH model. As visible from the phase diagram in figure 5, the Hubbard repulsion induces a transition from the quantum spin Hall phase to a Mott insulator with long-range magnetic order at a critical value U_c/t . The existence of this magnetic transition has first been demonstrated using mean-field theory [87].

Already for $U < U_c$, inside the correlated quantum spin Hall phase, the Hubbard interaction gives rise to the formation of local moments and substantial magnetic correlations. These correlations can be measured by the transverse spin structure factor [125, 126, 129]

$$S_{\text{AF}}^{xy} \equiv \sum_{\alpha} [S_{\text{AF}}^{xy}]^{\alpha\alpha}, \quad (25)$$

$$[S_{\text{AF}}^{xy}]^{\alpha\beta} = \frac{1}{L^2} \sum_{\mathbf{r}\mathbf{r}'} (-1)^{\alpha} (-1)^{\beta} \times \langle \Psi_0 | S_{\mathbf{r}\alpha}^{+} S_{\mathbf{r}'\beta}^{-} + S_{\mathbf{r}\alpha}^{-} S_{\mathbf{r}'\beta}^{+} | \Psi_0 \rangle,$$

and, similarly, by the longitudinal spin structure factor $S_{\text{AF}}^{zz} \equiv \sum_{\alpha} [S_{\text{AF}}^{zz}]^{\alpha\alpha}$ with

$$[S_{\text{AF}}^{zz}]^{\alpha\beta} = \frac{1}{L^2} \sum_{\mathbf{r}\mathbf{r}'} (-1)^{\alpha} (-1)^{\beta} \langle \Psi_0 | S_{\mathbf{r}\alpha}^{z} S_{\mathbf{r}'\beta}^{z} | \Psi_0 \rangle. \quad (26)$$

Here \mathbf{r}, \mathbf{r}' are vectors that indicate unit cells of the honeycomb lattice, $\alpha, \beta \in \{A, B\}$ are sublattice indices,

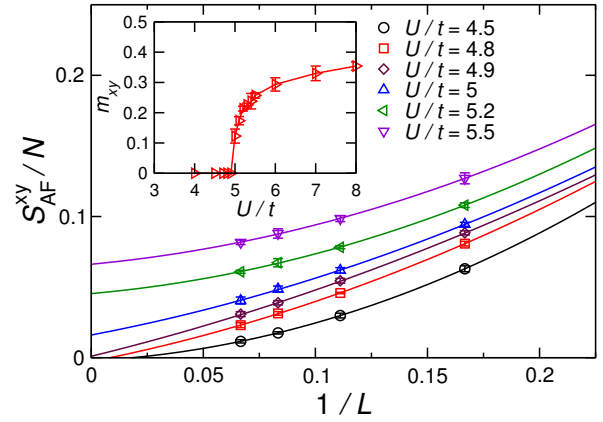


Figure 9. Finite-size scaling of the rescaled magnetic structure factor S_{AF}^{xy}/N (25) in the KMH model with $\lambda_{\text{SO}}/t = 0.1$ and for different values of U/t [126]. The quantity S_{AF}^{xy}/N extrapolates to zero in the quantum spin Hall phase and to a finite value in the magnetic phase; the critical value is $U_c/t = 4.95(5)$. Inset: order parameter m^{xy} as obtained from the size-extrapolated values. (Reprinted with permission from [126]. Copyright 2012 by the American Physical Society).

$(-1)^{\alpha} = 1 (-1)$ for $\alpha = A (B)$, and the trace of the 2×2 matrices is taken.

Quantum Monte Carlo results for the quantity S_{AF}^{xy}/N (with $N = 2L^2$ being the number of lattice sites), which is related to the transverse magnetization by $m_{xy}^2 = S_{\text{AF}}^{xy}/N$, are shown in figure 9 for different values of U/t and for $\lambda_{\text{SO}}/t = 0.1$ [126]. Up to $U/t = 4.9$, magnetic correlations are substantial on small length scales but the structure factor extrapolates to zero in the thermodynamic limit $L \rightarrow \infty$. For $U/t \geq 5$, long-range magnetic order is found. The critical value can be estimated as $U_c/t = 4.96(4)$ [126], and the transition is well visible from the magnetization results displayed in the inset of figure 9. A similar analysis for S_{AF}^{zz}/N reveals that no long-range order exists up to very large values of U/t [126], in contrast to predictions of longitudinal order based on cluster calculations [132]. A very similar picture arises for other values of λ_{SO}/t [126]. At first sight, the increase of U_c with increasing λ_{SO} visible in figure 5, and observed in several other works [87, 94, 125, 129, 131–133, 137], may be attributed to the increase of the spin-orbit gap. However, since U_c also increases from $U_c/t = 5.70(3)$ at $\lambda_{\text{SO}}/t = 0.2$ [127] to $U_c/t = 6.5(1)$ at $\lambda_{\text{SO}}/t = 0.3$ [125] even though the minimal gap at the M points remains constant [87], the origin of the increase of U_c is instead expected to be related to the competition between kinetic energy and magnetic order.

The fact that the magnetic ordering occurs in the xy direction can be understood from an effective spin model derived in the limit $U/t \rightarrow \infty$ where charge degrees of freedom are frozen out [87]. The spin Hamiltonian takes the form [31, 87, 137]

$$H_{\text{KMH}}^{\infty} = J \sum_{\langle ij \rangle} \mathbf{S}_i \cdot \mathbf{S}_j + J' \sum_{\langle\langle ij \rangle\rangle} (S_i^z S_j^z - S_i^x S_j^x - S_i^y S_j^y). \quad (27)$$

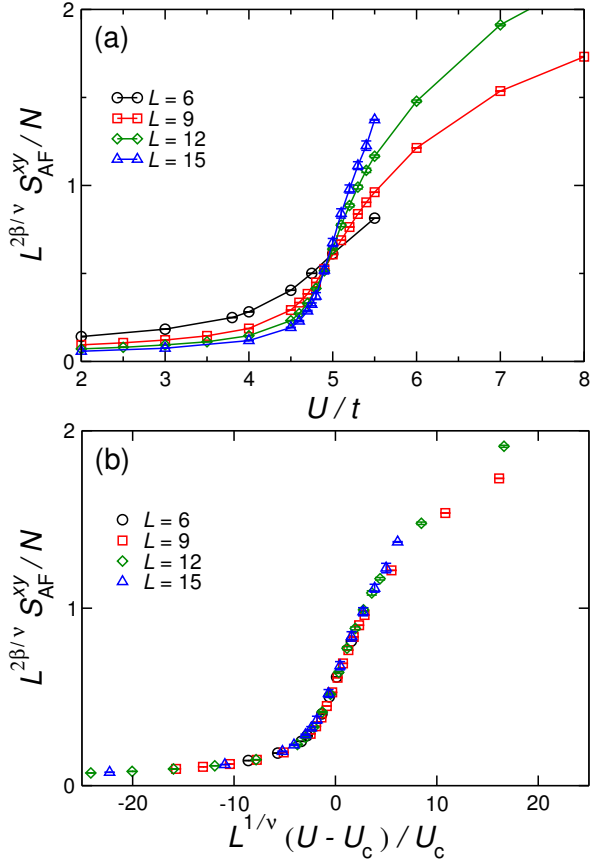


Figure 10. (a) Rescaled transverse magnetic structure factor S_{AF}^{xy}/N , see (25), as a function of U in the KMH model with $\lambda_{SO}/t = 0.1$. Assuming 3D XY behaviour and using the critical exponents of the 3D XY model [142], a clean intersection of curves for different system sizes L at the critical point $U_c/t = 4.96(4)$ is obtained. (b) Scaling collapse of $L^{2\beta/\nu} S_{AF}^{xy}/N$ as a function of $L^{1/\nu} (U - U_c)/U_c$ using $U_c/t = 4.96(4)$ and 3D XY exponents. (Reprinted with permission from [126]. Copyright 2012 by the American Physical Society).

The first term is an antiferromagnetic coupling between neighbouring lattice sites emerging from nearest-neighbour hopping ($J = 4t^2/U$), whereas the second term originates from the spin-orbit interaction ($J' = 4\lambda_{SO}^2/U$) and couples next-nearest-neighbour sites ferromagnetically in the xy direction and antiferromagnetically in the z direction. Hence, at least for large U/t , the KMH model corresponds to a frustrated spin model with respect to the z component of spin, but allows for nonfrustrated magnetic order in the xy direction. Exact numerical results [125, 126, 129] confirm this strong-coupling picture. For the parameter range of figure 5, no order in the z direction was found down to $\lambda_{SO}/t = 0.002$ [126].

Considering the spin-conserved case ($\lambda_R = 0$), the spin-orbit coupling in the KMH model reduces the spin symmetry from $SU(2)$ to $U(1)$. Therefore, the magnetic transition is expected to be in the universality class of the 3D XY model [125, 128, 138]. The quantum Monte Carlo method permits one to test this conjecture. Assuming that

the transition is of the 3D XY type, the order parameter S_{AF}^{xy}/N is expected to fulfil the scaling equation [126]

$$S_{AF}^{xy}/N = L^{-2\beta/\nu} f_1[(U - U_c)L^{1/\nu}] \quad (28)$$

where $z = 1$, $\nu = 0.6717(1)$ and $\beta = 0.3486(1)$ are the critical exponents of the 3D XY model [142]. In particular, (28) implies that at the critical point, $U = U_c$, S_{AF}^{xy}/N should become independent of the system size L . As illustrated in figure 10(a) for $\lambda_{SO}/t = 0.1$, the numerical results [142] indeed reveal the expected behaviour, showing a well-defined intersection of curves for different L at the critical point. Moreover, a clean scaling collapse is obtained upon rescaling the U axis according to (28), see figure 10(b). The 3D XY scaling of S_{AF}^{xy}/N has also been verified for other values of λ_{SO}/t [126, 127], as well as for the spin gap Δ_s [126]. The 3D XY criticality can be expected to be generic for quantum spin Hall models with conserved spin. If spin is not conserved, the symmetry is reduced to the Z_2 Ising universality class, allowing magnetic order at finite temperatures.

At the magnetic transition, time-reversal symmetry—underlying the topological protection of the quantum spin Hall state—is broken. Therefore, a change of the topological invariant from nontrivial to trivial does not require the closing of any gaps. Indeed, quantum Monte Carlo simulations reveal only a slight dip of the single-particle gap near the critical point, see figure 6. Very similar behaviour is also found in mean-field theory, see inset of figure 6. On the other hand, the spin gap Δ_s does close at the magnetic transition, corresponding to the condensation of magnetic excitons [126, 127, 138]. For $U < U_c$, excitons have a finite energy, and can be used in combination with π fluxes (see section 6) to construct quantum spin models with tunable interactions [127]. The coupling between the helical edges states and the magnetic excitons at the critical point was recently discussed by Grover and Vishwanath [143].

An interaction-driven magnetic transition has also been reported for the BHZH model [94, 97, 98]. Whereas existing work has focused on equal bandwidths for hopping via the s and p orbitals ($t_{ss} = t_{pp}$), a much richer picture can be expected for more general parameters. In the absence of the complex spin-orbit coupling ($t_{sp} = 0$), the BHZH model reduces to the two-band Hubbard model. The latter has been studied intensely as it may describe consecutive Mott transitions within the heavier and lighter band [144–147]. The interplay of orbital-selective Mott transitions and spin-orbit coupling represents a fascinating topic for future research. The SI model (9) is expected to undergo a magnetic transition in the Ising universality class if the spin-orbit coupling is not too large [102], see also figure 11.

Time-reversal symmetry is a key concept for the understanding of topological insulators, and underlies many of their properties. Remarkably, topological insulators can exist even in systems where time-reversal symmetry is broken by long-range magnetic order. As first discussed

by Mong *et al* [141] for three dimensions, a topological state with protected edge states can exist in the absence of time-reversal symmetry Θ if $S = \Theta T_{1/2}$ remains conserved, where $T_{1/2}$ is a translation symmetry defined by the unit cell of magnetic order. A simple example is given by an antiferromagnet in which the magnetic order leads to a doubling of the unit cell. Three-dimensional antiferromagnetic topological insulators may be realized in GdBuOt [141] as well as with ultra-cold atoms [80]. In two dimensions, the existence of edge states protected against disorder has been shown to additionally require spin conservation [148]. According to Guo *et al* [148], nonmagnetic or magnetic staggered potentials can drive the noninteracting BHZ model into a topological phase. Surprisingly, for the same model, a correlated topological phase with coexisting magnetic order has recently been reported by Yoshida *et al* [101]. If this phase indeed exists, it is interesting to understand why it is absent in the KMH model. However, another possibility is that the coexistence is due to the fact that the dynamical mean-field theory applied in [101] does not allow for magnetic order in the xy direction (as preferred for systems with spin-orbit coupling). Indeed, at the level of static mean-field theory, two different critical points can be observed when decoupling the interaction in terms of the magnetization in the z and the xy direction, respectively. Phases in which topological order coexists with magnetic order, for example *topological spin density waves*, have also been found in the interacting, spinful Haldane model (also known as the topological Hubbard model) [149–151]. In contrast to the BHZH model of [101], the topological Hubbard model breaks time-reversal symmetry from the outset.

A related theoretical problem, yet with important differences, is that of the Haldane-Hubbard model defined in (5). Without spin-orbit coupling ($t_2 = 0$), the nearest-neighbour repulsion drives a second-order transition to a charge-density-wave insulator that spontaneously breaks inversion symmetry [35, 152, 153]. The two degenerate ground states have all electrons on either the A or the B sublattice. Because inversion symmetry is in principle not relevant for the stability of the topological state of the Haldane model, in contrast to the role of time-reversal symmetry for the quantum spin Hall state, the question how the transition will occur for nonzero t_2 is very interesting. This problem was studied using mean-field theory, exact diagonalization, and constrained-path Monte Carlo simulations [90–92]. Although the results do not fully agree, there is evidence that the Chern number changes from nontrivial to trivial, and that this change and the onset of long-range charge order can either coincide, or happen in two distinct transitions. It is not yet clear if a gap closes at the critical point. However, because the topological phase does not rely on inversion symmetry, and the topological protection is therefore not destroyed by the charge order, one may expect to see the closing of an excitation gap at the

point where the Chern number changes. This appears to be confirmed by recent results [92], which relate the closing of the first excitation gap ($E_1 - E_0$, the difference between the two lowest eigenvalues) to a topologically protected level crossing that exists even in finite systems.

4.3.2. Symmetry-conserving transitions The magnetic and charge-density-wave transitions discussed above involve a well-defined, local order parameter, and in general may or may not coincide with the destruction of topological order (in the sense of a nonzero spin Chern or Chern number, respectively). Here the possibility of interaction-driven transitions without symmetry breaking is discussed, including transitions across which topological order either remains or emerges.

In the context of the KMH model, the possible quantum spin liquid phase shown in figure 5 has received a lot of attention. Quantum Monte Carlo results suggest that this phase has nonzero single-particle and spin gaps, but does not break any symmetries [81]. Furthermore, numerical results are compatible with a closing of the single-particle and spin gaps at the transition to the quantum spin Hall state, which suggests that the two phases are not adiabatically connected [125, 126]. However, despite the remarkable system sizes accessible in numerical simulations, the length scales for spin correlations are still not under control [126, 139], making extrapolations to the thermodynamic limit very delicate. The existence of the quantum spin liquid phase in the Hubbard model ($\lambda_{\text{SO}} = 0$) has recently been challenged based on quantum Monte Carlo results on lattices with up to 36×36 unit cells [139]. Signatures of the spin liquid phase in the KMH model have also been reported from quantum cluster simulations [131, 132], although the latter cannot describe a true spin liquid phase because of the inherent breaking of translation symmetry; instead, the observed paramagnetic insulator may be regarded as a valence bond solid. Furthermore, the quantum spin liquid phase of the KMH model has been related to a topological Mott insulator [135]. Because the KMH and SI models coincide for $\lambda_{\text{SO}} = t_1 = t_2 = 0$, the same phase may also be expected to exist in the SI model. At finite spin-orbit coupling, the frustrated spin exchange interactions of the SI model (see below) may even provide a more favourable setting for such a state. A review of the connections between spin liquids and topological insulators has been given by Fiete *et al* [76].

For two-dimensional models with explicit spin-orbit coupling, the possibility of a topological Mott insulator has first been discussed by Rachel and Le Hur [87], following an earlier suggestion by Pesin and Balents [36]. Within a slave-rotor approach to the KMH model, the charge degrees of freedom can be gapped out, whereas the spin degrees of freedom inherit the topological band structure, and hence preserve time-reversal symmetry [87]. Such an interaction-generated state is expected to have topological

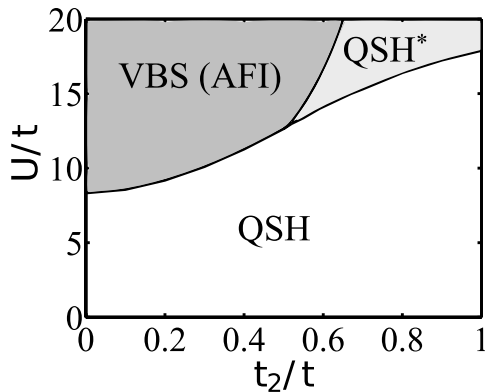


Figure 11. Mean-field phase diagram of the SI model, showing a quantum spin Hall phase (QSH), a valence bond solid (VBS), and a fractional QSH* phase [102]. (Adapted with permission from [102]. Copyright 2012 by the American Physical Society).

order. For the KMH model, the corresponding phase was suggested to lie in between the quantum spin Hall and antiferromagnetic Mott insulator regions of figure 5, but is not visible in numerical simulations [126]. Its absence can be attributed to the role of gauge fluctuations in two dimensions [87]. A topological Mott insulator with gapped charge *and* spin excitations in the KMH model [135]—presumably stable with respect to gauge fluctuations—was argued to be related to the quantum spin liquid phase shown in figure 5. Transitions from topologically trivial to nontrivial states upon increasing the Hubbard repulsion U have also been reported for the BHZH model [98, 100] and for a bilayer square-lattice model [110], in both cases starting with band parameters outside the respective quantum spin Hall phase. Of particular interest is the fact that such a transition can be either of the mean-field type (via a renormalization of single-particle parameters), or driven by quantum fluctuations [100].

A particularly interesting, strongly correlated topological phase has been argued to exist in the SI model (9). Following the suggestion of a strongly correlated quantum spin Hall phase resulting from the coupling to a dynamical Z_2 gauge field by Ran *et al* [154], Rüegg and Fiete [102] used a self-consistent Z_2 slave-spin mean-field theory to demonstrate the existence of the so-called QSH* phase in the SI model. Their phase diagram, reproduced in figure 11, exhibits an extended regular QSH phase, and a valence bond solid at large U/t . The latter is expected to become an antiferromagnetic Mott insulator (AFI) phase similar to figure 5 when the possibility of time-reversal symmetry breaking is added to the theory [102]. For large spin-orbit coupling t_2 and large Hubbard U , the QSH* phase emerges. It has been pointed out that because the QSH–QSH* transition corresponds to an order-disorder transition of the slave spins [102], the QSH* phase should be considered an *orthogonal metal* rather than a Mott insulator [155].

According to [102], the QSH* phase is characterized

by a bulk band gap, and protected helical edge states for charge and spin excitations. It supports fractional, bosonic quasi-particle excitations with semionic mutual braiding statistics [102]. The phase does not break any symmetries, but has a four-fold topological degeneracy on a torus [102]. It is thus topologically ordered in the sense of section 1, and hence distinguished from the QSH phase by the presence of long-range quantum entanglement [45]. Fractional time-reversal invariant liquids will be further discussed in section 4.5. Because of the strong interactions, the edge states are expected to be strongly correlated [102], leading to a suppression of the Drude weight in agreement with results for other models (section 5.2).

The reliability of the mean-field results in [102] is not yet clear. Moreover, because spin is not conserved, the SI model can presently not be investigated by quantum Monte Carlo methods. This situation has motivated two recent studies of the limit $U/t = \infty$, in which an effective spin model can be derived [31, 32]. It has the form [31, 32]

$$H_{\text{SI}}^{\infty} = J_1 \sum_{\langle ij \rangle} \mathbf{S}_i \cdot \mathbf{S}_j + J_2 \sum_{\langle\langle ij \rangle\rangle} \mathbf{S}_i \cdot \mathbf{S}_j - J_3 \sum_{\langle\langle ij \rangle\rangle} (\mathbf{S}_i \cdot \mathbf{S}_j - 2S_i^w S_j^w). \quad (29)$$

Here the exchange constants are $J_1 = 4t^2/U$, $J_2 = 4t_1^2/U$, and $J_3 = 4t_2^2/U$. The coupling J_2 was neglected in [31]. Importantly, the term $S_i^w S_j^w$ depends on the link that connects sites i and j , leading to frustration and the absence of any preferred direction for magnetic order [31]. In contrast, in the $U/t = \infty$ limit of the spin-conserving KMH model, (27), order in the spin- z direction is frustrated, but easy-plane order is not. The Hamiltonian (29) has close connections to the Kitaev-Heisenberg model [29, 30], an exactly solvable model with a spin liquid ground state.

For small values of J_2 , the model (29) undergoes transitions from stripe order to Néel order to spiral order upon increasing J_3 from negative to positive values [31, 32]. For the repulsive SI model, the transition from Néel to spiral order is of particular interest, and has been interpreted as a strong-coupling signature of the VBS (or AFI) to QSH* transition [31, 32]. A magnetic transition from the QSH* to the spiral state is expected to occur with increasing U/t [31]. The spin-nonconserving SI model hence appears to describe phenomena beyond the numerically studied KMH model with $\lambda_{\text{R}} = 0$, although incommensurate order has also been predicted for the latter analytically [137]. An interesting question for future research is if fractional topological states and exotic magnetic states can also occur in the KMH model with $\lambda_{\text{R}} \neq 0$ [31]. The corresponding spin Hamiltonian has been derived in [31].

4.4. Interaction-driven topological insulators

Spin-orbit coupling plays a crucial role for topological insulators [11, 12, 23]. In general, materials with heavy

atoms are required for the effects of spin-orbit coupling to be observable. On the theoretical side, the existence of topological phases in models with intrinsic spin-orbit coupling can be understood in the framework of topological band theory [14] without considering electronic correlations. A completely different approach to create quantum spin Hall phases is based on the theoretical concept of a *topological Mott insulator*, a state with an interaction-generated band gap and protected edge states [35]. In addition to providing a much richer theoretical setting to study correlated topological phases, this concept promises the existence of topological phases in a wider range of materials by abandoning the need for strong intrinsic spin-orbit coupling.

Raghu *et al* [35] considered an extended Hubbard model on the honeycomb lattice with the usual nearest-neighbour hopping term (see (1)) as well as onsite (U), nearest-neighbour (V_1) and next-nearest-neighbour (V_2) repulsion in the form of density-density interaction terms. In the spinless case, the repulsion V_2 frustrates the charge-density-wave order driven by V_1 , and a mean-field treatment suggests that large values of V_2 lead to a state with spontaneously broken time-reversal symmetry characterized by a nonzero, imaginary value of the bond order parameter $\chi_{ij} = \langle \hat{c}_i^\dagger \hat{c}_j \rangle$ [35]. This state is fully equivalent to the integer quantum Hall state of the Haldane model [9]. In the spinful case, the nonzero bond order parameter can either have the same or opposite signs for the two spin directions. The former case leads to a quantum anomalous Hall state, whereas the latter case corresponds to a quantum spin Hall state resulting from a dynamically generated spin-orbit coupling that breaks the $SU(2)$ spin symmetry [35, 156]. At the mean-field level, the quantum Hall and quantum spin Hall states are degenerate. Taking into account quantum fluctuations within the random-phase approximation reveals that the quantum spin Hall state is favoured because of the existence of a Goldstone mode, and leads to the phase diagram shown in figure 12 [35]. In addition to the quantum spin Hall phase, the latter contains semimetal, spin-density-wave and charge-density-wave states. Similar results and the possibility of a spin-dependent Kekulé order parameter were discussed by Weeks and Franz [157]. In contrast to models with intrinsic spin-orbit coupling, the quantum spin Hall state from dynamical spin-orbit interactions is characterized by a local order parameter. Nevertheless, it will in general be necessary to calculate the topological invariant to distinguish such a state from one that has a nonzero order parameter but is topologically trivial. Whether the quantum spin Hall state arising from a dynamically generated spin-orbit coupling can be adiabatically connected to a noninteracting QSH state (or instead supports fractional excitations) is an open question. Finally, for spinless fermions on a honeycomb lattice with extended interactions, mean-field theory predicts the

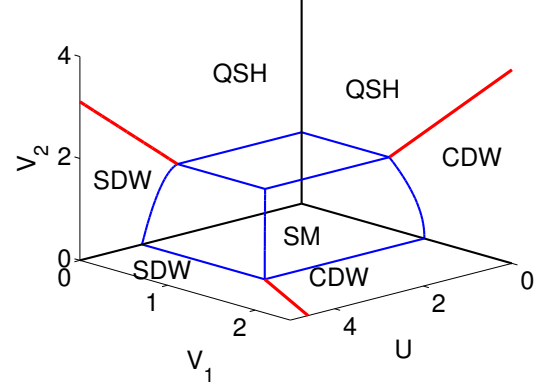


Figure 12. Mean-field phase diagram of the extended Hubbard model (with repulsions U , V_1 , V_2) on the honeycomb lattice [35]. The phases correspond to a semimetal (SM), charge-density-wave order (CDW), spin-density-wave order (SDW), and a quantum spin Hall state (QSH) emerging from dynamically generated spin-orbit coupling. (Reprinted with permission from [35]. Copyright 2008 by the American Physical Society).

existence of a quantum anomalous Hall phase [35, 68, 157]; the resulting order parameter is equivalent to the single-particle hopping terms in the Haldane model [9]. A possible realization with Rydberg atoms in an optical lattice is discussed in [68].

Interaction-driven topological states in models without intrinsic spin-orbit coupling have also been studied on the checkerboard [88], kagome [158, 159], and decorated honeycomb lattices [159]. Most importantly, these more complicated geometries support both Dirac band crossing points and quadratic band crossing points depending on the band filling in the noninteracting limit. For example, the low-energy physics on the kagome lattice is determined by a Dirac point for $n = 1/3$ and by a quadratic crossing point for $n = 2/3$. Both filling fractions support a quantum spin Hall phase in the presence of intrinsic spin-orbit coupling [103]. However, whereas topological order due to interaction-generated spin-orbit terms is the leading instability for $n = 2/3$, it competes with other ordering phenomena and requires strong interactions and fine-tuning in the case $n = 1/3$ due to the vanishing density of states at the Fermi level [159]. In principle, because these lattices support partially filled flat bands, the interacting models are good candidates for fractional topological phases. A topological phase arising from spontaneous ordering of complex orbitals has been found theoretically in a model of transition-metal heterostructures [58]. Importantly, in such multi-orbital models, topological order can emerge from purely local interactions, whereas nonlocal interactions are typically required for single-orbital models [58]. Another possible setting to observe interaction-generated topological states is stacked graphene [61, 62]. Finally, three-dimensional topological insulators can also be generated from interactions [160].

Topological states arising from electronic interactions have also been discussed in the context of systems with intrinsic spin-orbit coupling that undergo a Mott transition from a regular to an exotic quantum spin Hall phase of spinons, in which interaction-generated low-energy spin excitations inherit the topological band structure [36, 87, 135, 161], see also section 4.3. Alternatively, interactions can give rise to a transition from a nontopological state to an integer quantum spin Hall state, as in [98, 110], essentially via a renormalization of the effective spin-orbit coupling. In relation to fractional states to be discussed next, it is important to distinguish *fractionalized* and *fractional* topological insulators. The former are states with spin-charge separation but typically integer charge excitations, whereas the latter are states that exhibit charge fractionalization as in the fractional quantum Hall effect.

4.5. Fractional topological insulators

Given the close relation between integer quantum Hall states and quantum spin Hall insulators, Bernevig and Zhang [162] envisaged the possibility of fractional time-reversal invariant insulators arising from strong electronic interactions [162]. Levin and Stern [41] considered the case of independent fractional quantum Hall states for \uparrow and \downarrow spins, and established that the criterion for the existence of edge states protected by time-reversal symmetry is that σ_{xy}^s/e^* is odd, where e^* is the elementary charge of the fractional Hall state. However, a combination of two fractional quantum Hall states is not necessarily a topological insulator with protected edge modes, but can instead also lead to *fractional trivial insulators* with σ_{xy}^s/e^* even [41]. In the latter, edge modes can be gapped out by time-reversal invariant perturbations.

A lattice model that supports the integer quantum Hall effect without a magnetic field was introduced by Haldane [9], see (5). Analogous models for fractional quantum Hall states were discovered only recently, for example, in [39, 107, 163–167]. A common feature of such models is the existence of flat bands with a nonzero Chern number (so-called *Chern bands*) that mimic the Landau levels of more traditional fractional quantum Hall states observed in strong magnetic fields [3]. The flatness allows electronic interactions to be large compared to the kinetic energy but small compared to the band gap (thereby avoiding level mixing effects and allowing for a projection onto a single-band problem). A number of Haldane-like models with these properties were suggested [39, 150, 163–165], and the existence of a fractional quantum Hall phase was demonstrated in [39, 165, 168]. The prospect of fractional quantum Hall states without magnetic fields has also inspired the search for materials with partially filled Chern bands arising from spontaneous orbital order, see [40] and references therein. Similar to the case of topological Mott insulators (section 4.4), the necessary spin-orbit coupling (or spin-dependent magnetic flux) can arise from

interaction-induced spontaneous symmetry breaking [40]. An adiabatic connection between Chern insulators and the Hofstadter problem is discussed in [169], and a proof for an adiabatic connection between fractional Chern insulators and fractional quantum Hall states has been given in [170].

In the integer quantum Hall effect, the chemical potential lies in the gap between the highest filled and the lowest unfilled energy levels. As long as the energy scale for electronic interactions is smaller than the gap to excited states, interaction effects can be considered as a small perturbation. In contrast, electronic correlations are at the heart of fractional quantum Hall liquids and hence also fractional topological insulators; for a review see [3]. At the special filling fractions for which σ_{xy} exhibits a plateau, a family of ground states with well-defined topological degeneracy is spontaneously selected from the highly degenerate set of many-body states. This process is inherently nonperturbative, and the fractional state has quasiparticle excitations with fractional charge and fractional statistics. The extremely rich physics known from the fractional quantum Hall effect stimulates research on fractional topological insulators. A previously encountered example of such a fractional spin Hall liquid is the QSH* phase of the SI model [102], see section 4.3.

Neupert *et al* [124] considered the general case of a fractional liquid with time-reversal symmetry but no spin conservation. Such states (including the noninteracting, integer quantum spin Hall states) are described at low energies by Abelian Chern-Simons theories, whereas the special case with spin conservation is described by a $U(1) \times U(1)$ Chern-Simons or BF theory [77, 171]. If spin is not conserved, the existence of protected edge states can be related to a Z_2 invariant independent of σ_{xy}^s that reduces to the usual Z_2 index in the integer, noninteracting limit [124]. A general Chern-Simons theory of two-dimensional, time-reversal invariant insulators with Abelian quasiparticles and a classification of fractional topological insulators was given by Levin and Stern [172]. Recent work along these lines includes parton [173] and composite fermion [174] descriptions, the relation between fractional topological insulators and quantum Hall states in Landau levels [175], and an effective field theory of general fractional, two-dimensional topological insulators with spin-orbit coupling [176, 177]. Because the fractional states arise from strong interactions, topological order will typically compete with other many-body instabilities such as charge-density-wave formation. For Chern insulators, the stability of the topological state has been found to be enhanced by a certain amount of band dispersion or for bands with higher Chern numbers [178]. Finally, the experimental detection of fractional topological insulators, including the determination of the filling fraction from transport measurements, is discussed in [179].

An important open problem is the question under what circumstances two coupled fractional Hall liquids

form a fractional topological insulator with protected edge modes. The interactions between the two fractional states may completely destroy the insulating state, give rise to spontaneous breaking of time-reversal symmetry, or lead to novel, non-Abelian states [124]. It will also be interesting to see if the physics beyond the Laughlin states recently reported for Chern insulators [167, 180] carries over to fractional topological insulators. Most of the numerical work on fractional topological insulators so far relies on exact diagonalization, with an exponential scaling of computational effort with system size. A possible alternative is the use of tensor network states [181].

5. Edge correlation effects

The existence of metallic, protected edge states is one of the most obvious manifestations of the topological properties of quantum spin Hall systems [11, 12], and has played a crucial role for the experimental verification of the existence of topological insulators [20, 21]. The fundamental properties of these edge states can be understood in the noninteracting limit, as reviewed in section 3. Because of time-reversal symmetry, the edge states always exist as Kramers pairs, and electrons of opposite spin propagate in opposite directions along a given sample edge. For an odd number of such helical edge state pairs, time-reversal symmetry provides a protected, gapless crossing point [12]. In contrast, single-particle backscattering is possible for an even number of pairs, and the edge states are not protected [11, 12]. The parity of the number of edge state pairs can therefore be related to the Z_2 topological invariant [11].

Compared to the gapped bulk, electron-electron interactions can be expected to strongly affect the gapless edge states [79]. Most importantly, in the presence of interactions, inelastic scattering becomes possible, and is not forbidden by Kramers theorem, as it connects states of different energy [79]. Moreover, whereas time-reversal symmetry forbids elastic single-particle processes, two-particle backscattering is allowed even for a single Kramers pair. The possibility of such processes, which can spontaneously break time-reversal symmetry at the edge [78, 79], is a crucial difference to the quantum Hall effect, where counter-propagating states (and hence backscattering) are completely absent [120]. As pointed out in [78, 79], the qualitative, topological distinction between odd and even numbers of edge state pairs in the noninteracting case becomes a quantitative distinction (depending on the interaction strength) in the presence of correlations. However, as discussed below, for the class of models with conserved spin and without impurities, the topological protection and the bulk-boundary correspondence remain intact.

An odd number of Kramers edge state pairs, and hence a topologically protected quantum spin Hall state,

can be realized only at the boundary of a two-dimensional system [78], giving rise to the notion of a *holographic liquid* [78]. Hence, edge states of a quantum spin Hall insulator may be regarded and theoretically described (to a good approximation) as one-dimensional liquids that inherit their topological properties from the bulk [79, 121]. Similar to other quasi-one-dimensional systems such as quantum wires, quantum fluctuations play a key role in determining the physics of edge states. Consequently, whereas mean-field theory provided valuable insight into the effect of bulk correlation effects, it is insufficient for edge physics and in fact gives misleading results as a result of instabilities [138]. Similarly, given the non-Fermi liquid character of the metallic edge states, perturbative approaches fail. Instead, Luttinger liquid theory [182] provides a rather accurate description of many aspects [78, 79]. Although a strictly one-dimensional description seems justified by the exponential suppression of scattering to bulk states, signatures of the holographic nature of the helical edge states are visible as quantitative deviations from bosonization predictions [140].

In this section, an introduction to the helical Luttinger model is given [78, 79] (for a previous review see [14]), followed by a discussion of analytical and numerical results with an emphasis on theoretical aspects of the intensely studied integer quantum spin Hall insulators. A more experimentally oriented review of transport properties was given by Tkachov and Hankiewicz [183]. Other interesting developments not addressed in the following include Majorana edge states of topological superconductors [143], and edge states of fractional topological insulators [41, 179]. Finally, the stability of edge states in magnetically ordered topological insulators is discussed in [80, 141, 148–150].

5.1. Luttinger liquid description

The low-energy description of helical edge states in terms of Luttinger liquid theory was established in two early papers by Wu *et al* [78] and Xu and Moore [79]. The corresponding theory and hence the physics is independent of the particular model for the bulk as long there is an adiabatic connection to the noninteracting case. (For edge state theories of fractional topological insulators see [41, 124, 179].) However, details such as the number of edge states, the allowed interactions and the location of the crossing in momentum space are determined by the Z_2 topological invariant, the spin symmetry, the bulk band structure and the edge topology (for example, zigzag or armchair for honeycomb lattice models). For a generic topological insulator, the low-energy model for the edge states can be derived from Chern-Simons theory [79, 121], see also section 3.

In the following, a single pair of edge states is considered, assuming a geometry that is wide enough for the two edges to be independent. Correlation effects

on even numbers of edge state pairs, corresponding to a topologically trivial state in the noninteracting case, have been discussed by Xu and Moore [79]. Surprisingly, in this situation, the edge states can be stabilized against localization by interactions [79]. Effects of inter-edge tunnelling [99, 138, 184] will be addressed in section 5.2.

The following discussion follows Wu *et al* [78] (see also [14]). Assuming a system with periodic boundaries in the x direction and open boundaries in the y direction, and linearizing the edge dispersion as $\epsilon_\sigma(k) = \pm v_F(k - k_F)$, the free continuum theory takes the form

$$H_0 = v_F \int dx (\psi_{R\uparrow}^\dagger i\partial_x \psi_{R\uparrow} - \psi_{L\downarrow}^\dagger i\partial_x \psi_{L\downarrow}). \quad (30)$$

The helicity of the edge states is apparent from the existence of right moving electrons (R) with velocity v_F and only spin \uparrow , and left moving electrons (L) with velocity $-v_F$ and only spin \downarrow . The spin directions can be defined with respect to an arbitrary quantization axis even if spin is not conserved. The Fermi velocity v_F is related to the bulk band gap and the edge topology, but analytical expressions for specific models are in general not known (see, for example, [185]). Because of the correspondence between the direction of motion and spin, a spin index is not required, and drops out of the effective low-energy Luttinger liquid theory (see below). An interesting consequence of the reduced number of degrees of freedom compared to ordinary Luttinger liquids is the predicted possibility to observe fractional charges [186].

To derive the low-energy model, it is necessary to consider the possible interactions. Elastic perturbations which are odd under time reversal, most importantly single-particle backscattering, are not allowed. Inelastic single-particle scattering is allowed, but requires a spin flip. It can arise, for example, from magnetic impurities, Rashba coupling in combination with phonons [187], or a coupling to spin-1 bosons (for example, spin fluctuations [140]). Forward scattering as well as elastic or inelastic two-particle processes are generally allowed [78, 79]. Although a discussion of scattering processes based on the single-particle picture is physically intuitive, a many-body formulation [79] is more appropriate for interacting systems, and leads to the same low-energy Luttinger model. A continuum theory of helical edge states was presented in [188]. Bosonization results for non-helical one-dimensional systems with spin-orbit coupling can be found in [189, 190].

Forward scattering is described by [78]

$$H_{\text{fw}} = g \int dx \psi_{R\uparrow}^\dagger \psi_{R\uparrow} \psi_{L\downarrow}^\dagger \psi_{L\downarrow}. \quad (31)$$

In clean systems, the most important two-particle term is umklapp scattering (i.e., backscattering from a periodic lattice potential), given by [78]

$$H_{\text{um}} = g_u \int dx e^{-i4k_F x} \psi_{R\uparrow}^\dagger(x) \psi_{R\uparrow}^\dagger(x+a) \times \psi_{L\downarrow}(x+a) \psi_{L\downarrow}(x) + \text{H.c.} \quad (32)$$

Whereas H_{fw} is generically present in helical liquids, the umklapp term only plays a role at half filling ($4k_F = 2\pi l$, l integer) and in the presence of spin-nonconserving terms in the Hamiltonian, such as the Rashba spin-orbit interaction [191]. It is therefore generically absent in models with $U(1)$ spin symmetry, even at half filling. Two-particle backscattering can also arise from magnetic impurities [78, 192–194] or quenched disorder [12, 78], see section 5.2. Finally, in systems without spin conservation, combined single-particle forward- and backscattering can become important [96].

Under the assumption that the edge states remain quasi-one-dimensional, interaction effects can be studied in the powerful framework of bosonization. If only forward scattering is allowed, electron-electron interactions can be accounted for by the Luttinger liquid parameters $K = \sqrt{(v_F - g)/(v_F + g)}$ and $v = \sqrt{v_F^2 - g^2}$ (these expressions are valid for $g \ll v_F$). The corresponding helical Luttinger model reads

$$H_{\text{HL}} = \frac{v}{2} \int dx [K^{-1}(\partial_x \phi)^2 + K(\partial_x \theta)^2], \quad (33)$$

where $\phi = \phi_R + \phi_L$ and $\theta = \phi_R - \phi_L$. For a given spin direction, only one chirality is allowed, in contrast to a regular Luttinger liquid where for each spin direction there are left and right moving electrons.

Because umklapp- and backscattering are excluded, the quadratic and hence exactly solvable Luttinger model (33) describes correlated but metallic helical edge states, as realized in a number of spin-conserving theoretical models without disorder. Electron-electron interactions lead to a change of the parameters K and v . Generally, $K = 1$ and $v = v_F$ for noninteracting electrons, and $K < 1$ ($K > 1$) for repulsive (attractive) interactions. However, no quantum phase transitions occur, and all correlation functions decay with power laws with exponents determined by K . Explicitly, the equal-time correlation functions can be derived as

$$S^{xx}(r) = \langle S^x(r) S^x(0) \rangle \sim \frac{1}{r^{2K}} \cos(2k_F r), \quad (34)$$

$$S^{zz}(r) = \langle S^z(r) S^z(0) \rangle \sim \frac{1}{r^2},$$

$$N(r) = \langle n(r) n(0) \rangle \sim \frac{1}{r^2},$$

$$P(r) = \langle \psi_{R\uparrow}(r) \psi_{L\downarrow}(r) \psi_{R\uparrow}^\dagger(0) \psi_{L\downarrow}^\dagger(0) \rangle \sim \frac{1}{r^{2/K}},$$

corresponding to transverse spin, longitudinal spin, charge and pairing correlations, respectively. The results in (34) imply that transverse spin correlations (described by $S^{xx}(r)$) are the slowest decaying correlations for repulsive interactions, whereas pairing correlations $P(r)$ dominate for attractive interactions. The longitudinal spin correlations $S^{xx}(r)$ (here $S^{zz} \neq S^{xx}$ reflects the broken $SU(2)$ spin symmetry in the presence of spin-orbit coupling) and charge correlations $N(r)$ decay exactly as in a Fermi liquid. Finally, only $S^{xx}(r)$ depends

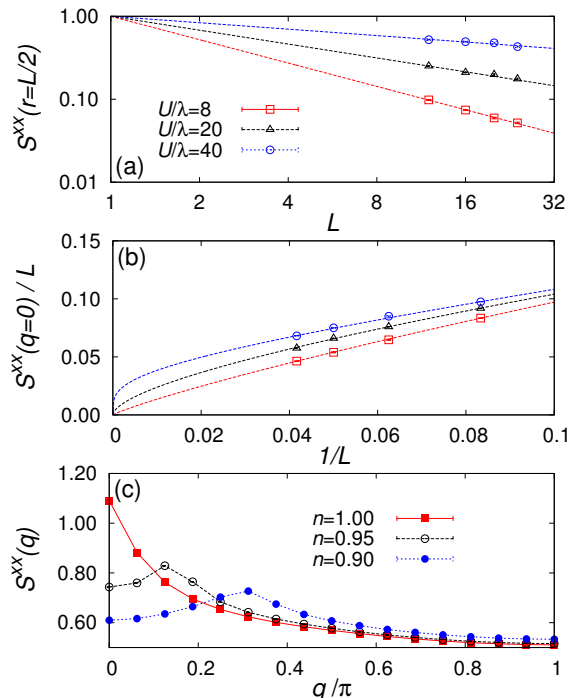


Figure 13. (a) Transverse spin correlator for different interaction strengths U/λ (λ : spin-orbit coupling), showing a power-law decay with an interaction-dependent exponent in accordance with (34). Lines are fits to the form A/r^η . Data are normalized to 1 at $r = 1$ for comparison. (b) Renormalized transverse spin structure factor at $q = 0$, showing the absence of long-range magnetic order in the thermodynamic limit. Lines are fits to the form $S^{xx}(q = 0)/L = b/L + c/L^\eta$, with η taken from (a). (c) Transverse spin structure factor at $U/\lambda = 8$ for different band fillings n . All results were obtained from zero-temperature quantum Monte Carlo simulations of an effective model with Hubbard interactions only at the edge of a zigzag ribbon. Data taken from [140].

on the Fermi momentum via the term $\cos(2k_F r)$, which can be related to spin-flip processes [140]. Whereas a nonlocal electron-electron interaction of finite range is qualitatively equivalent to the local interaction considered here, correlation functions deviate from the power-law Luttinger liquid form in the case of a long-range Coulomb potential [195, 196].

The bosonization predictions (34) have been tested numerically by considering the quantum spin Hall phase of microscopic, interacting models. To verify the characteristic interaction-dependent power-law decay of transverse spin and pairing correlation functions, a hallmark feature of one-dimensional liquids predicted by (34), rather large system sizes are required. Existing work along these lines is based on quantum Monte Carlo simulations of the KMH model [129], and of an effective model that takes into account electron correlations only at the edge [125, 140]. This approach is justified by the minor role of bulk interactions in the topological band insulator phase, as discussed in section 4. The effective model allows one to access large system sizes without any further approximations. (The results shown in [125, 140] were

obtained with an incorrectly implemented bulk Green function, and are therefore not for the KM model but for a different model of a quantum spin Hall insulator. However, using the KM Green function leads to very similar results, and none of the conclusions are affected, see errata of [125, 140]. In the following, figure 15 shows results for the KM model with edge interactions, whereas figures 13, 14, 18 correspond to previously obtained results for the alternative model.)

Results for $S^{xx}(r)$ are reproduced in figure 13(a) [140]. For a local Hubbard interaction, the forward scattering matrix element g depends on U , whereas the Fermi velocity is determined by the spin-orbit gap and hence by λ_{SO} . The effective interaction strength for the edge states is therefore set by the ratio U/λ_{SO} [140]. Figure 13(a) reveals that transverse spin correlations $S^{xx}(r)$ decay increasingly slower with increasing U/λ_{SO} , corresponding to a reduction of K in (34). All other correlation functions decay much faster [140]. Similar results have been obtained in a full bulk calculation of the KMH model [129, 130]. Despite the strongly enhanced transverse spin correlations, the Luttinger model predicts the absence of long-range order. This prediction is consistent with the finite-size scaling of the spin structure factor shown in figure 13(b). Figure 13(c) confirms the doping dependence of $S^{xx}(r)$ by showing its Fourier transform (the spin structure factor) at different particle densities. Away from half filling ($n = 1$, $k_F = \pi$), the $\cos(2k_F r)$ factor in (34) becomes visible. From the numerical results, and given the absence of logarithmic corrections to (34), the Luttinger parameters K and v can be determined using finite-size scaling. The results in figure 14 demonstrate a strong suppression of K from its noninteracting value $K = 1$, and a slight renormalization of the velocity in agreement with [131, 132]. The parameter K has also been determined from quantum Monte Carlo simulations of the KMH model by fitting power laws to correlation functions at a fixed system size [129], see figure 17. The renormalization of the velocity v was also studied in [132].

While the numerical value of K for given microscopic parameters U and λ_{SO} will depend on the details of the model, repulsive interactions generically lead to dominant $2k_F$ transverse spin fluctuations on helical edges [78, 79, 125, 129, 138, 140]. In the light of the bulk results discussed in section 4, transverse spin correlations are therefore a hallmark feature of correlated topological insulators. This finding is expected to hold even in the presence of Rashba coupling, as long as interactions are not too strong (see below). Although mean-field theory is not appropriate to describe correlated edge states, it does provide some insight into the differences between bulk and edge correlations. For a system with periodic boundaries, mean-field theory gives a finite critical value U_c at which the topological band insulator undergoes a quantum phase transition to a

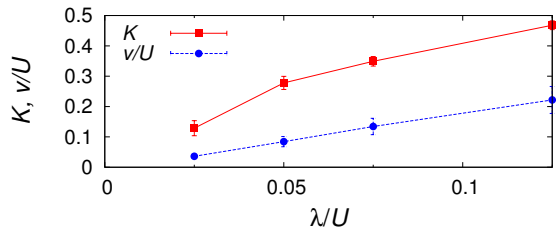


Figure 14. Luttinger liquid parameters K and v for an effective model of helical edge states, as obtained from quantum Monte Carlo simulations and finite-size extrapolation. Data taken from [140].

magnetic Mott insulator [87], see inset of figure 6. In contrast, a system with edges is unstable toward the opening of a gap due to a nesting-related, logarithmically diverging susceptibility, and shows a gapped magnetic state with long-range order, $\langle S^{xx} \rangle \neq 0$, for any finite U [138]. This so-called edge magnetism has been studied in the context of graphene [197–200]. Lee [138] has shown that for weak enough interactions, taking into account fluctuations around the mean-field saddle point restores the expected power-law decay at the edges. Although long-range order is absent, exact numerical results for the KMH model expose that magnetic correlations are still strongest at the edge, and decay quickly with the distance from the edge [129].

The effective model with interactions only at the edge sites provides a faithful description of the low-energy physics inside the quantum spin Hall phase [125, 140]. In addition to capturing the power-law decay of correlations expected from Luttinger liquid theory, this approach also permits one to calculate dynamical correlation functions on large systems. Figure 15(a) shows the single-particle spectral function of the KMH model with edge Hubbard interactions on a zigzag ribbon at $\lambda_{\text{SO}}/t = 0.2$ and $U/t = 2$. As in the noninteracting case (figure 4(a)), there is a gapless crossing point at $k = \pi$. The absence of any features related to spin-charge separation is a generic feature of one-dimensional systems with spin-orbit coupling [189]. The single-particle spectrum of a correlated helical liquid has also been obtained with cluster dynamical mean-field theory on zigzag and armchair edges [131], see figure 16, for the KMH model using the variational cluster approach [132], and for the BHZH model [96, 98, 99]. The real-space Green function of the helical Luttinger model has been calculated analytically [201].

Whereas dynamical two-particle correlation functions are not reliably accessible with cluster methods [131, 132] and difficult to obtain within bosonization, they can be calculated with high momentum resolution using quantum Monte Carlo simulations of the effective model [125, 140]. Figure 15 shows results for the KMH model with edge Hubbard interactions. The charge structure factor in figure 15(b) and the longitudinal spin structure factor in figure 15(c) are characterized by a linear mode at long wavelengths that has the same velocity as the edge state

visible in the single-particle spectrum shown in figure 15(a). The corresponding spectral weight is much smaller in the charge channel than in the spin channel. The linear mode is related to spin-conserving excitations within the helical states, whereas excitations at higher energies involve bulk states. The transverse spin structure factor shown in figure 15(d) involves spin flips—connecting the two helical edge modes—and therefore exhibits a continuum of low-energy excitations near $q = 0$ [140].

As confirmed by the explicit numerical calculations discussed in this section, for weak enough interactions, the fixed point described by the forward scattering model (33) qualitatively describes the physics of helical edges. As long as K does not fall below the respective critical values to be discussed below, the model remains valid even for systems with nonconserved spin [96], disorder [12, 78], or magnetic impurities [78, 192].

5.2. Strongly correlated regime

The robustness of helical edge states with respect to interactions is a result of time-reversal symmetry. At the time-reversal invariant momenta $k = 0, \pi$, the two edge modes necessarily have the same energy, $\epsilon_{\uparrow}(k) = \epsilon_{\downarrow}(k)$, so that the system is gapless. A gap in the edge states can arise from a breaking of time-reversal symmetry either globally (for example, due to spontaneous symmetry breaking and the onset of magnetic order in the bulk, see section 4), or only at the edge. In the latter case, the bulk remains a topological insulator, and the bulk-boundary correspondence breaks down [119, 202, 203]. This section explores the conditions for the occurrence of gapped edge states (such a gap is assumed to be small compared to the bulk band gap), and reviews the consequences of strong interactions—compared to the bulk gap—in systems that remain gapless for symmetry reasons. Quite generally, a gap in the edge states requires strong interactions, as measured by the Luttinger liquid parameter K . Evidence for strong interactions ($K \ll 1$) for a wide range of microscopic model parameters comes from numerical simulations [129, 140], see figures 14 and 17.

The impact of strong interactions can be analyzed by combining bosonization with the renormalization group method [78, 79]. Whereas forward scattering does not open a gap, backscattering terms become relevant for strong enough interactions [78, 79]. The umklapp term, important at half filling and for systems without spin conservation, becomes a relevant perturbation for $K < 1/2$ [78, 79, 138]. Backscattering due to quenched disorder leads to a gap if $K < 3/8$ [78, 79], whereas backscattering involving magnetic impurities becomes relevant for $K < 1/4$ [192, 193]. Finally, a gap in the edge states can also open in the presence of a lattice of magnetic impurities when $K < 1/2$ [193], and as a result of inter-edge tunneling and/or umklapp processes [99, 138, 184]. The helical liquid hence shows remarkable differences compared to ordinary

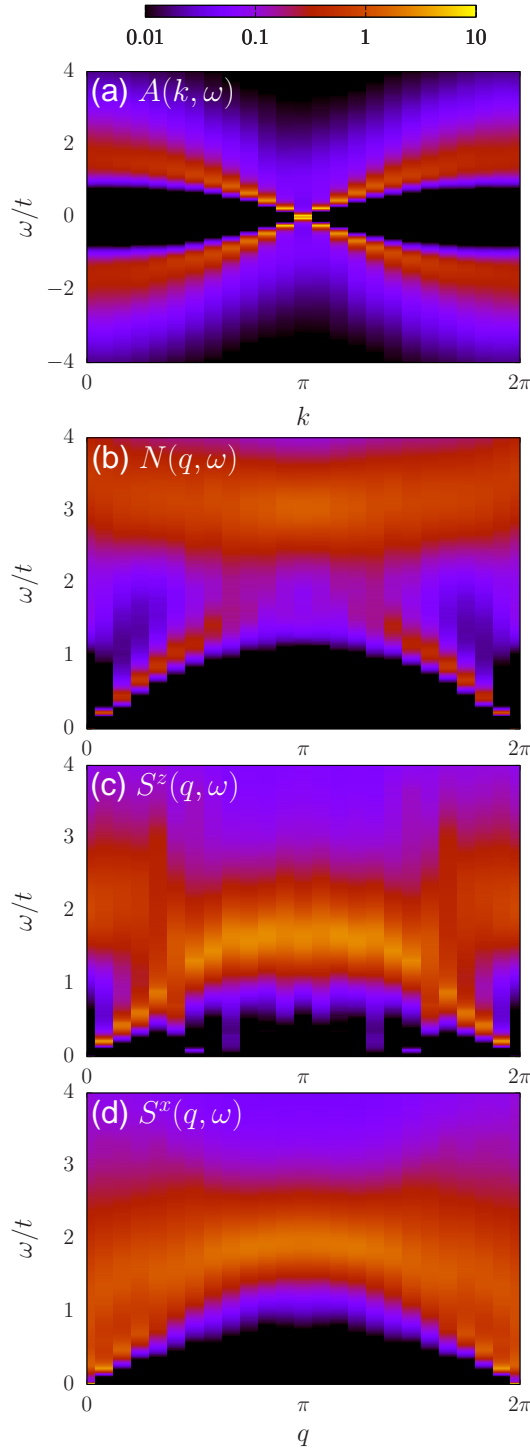


Figure 15. Dynamical correlation functions for (a) single-particle, (b) charge, (c) longitudinal spin, and (d) transverse spin excitations. Results obtained from zero-temperature quantum Monte Carlo simulations of the KMH model on a 24×64 zigzag ribbon with a Hubbard U only at the edge sites [125, 140]. Here $U/t = 2$ and $\lambda_{\text{SO}}/t = 0.2$.

Luttinger liquids. In the latter, if $K_\rho < 1$, transport is completely blocked at $T = 0$ by either disorder [122] or a single magnetic impurity (the Kondo problem) [204].

In contrast, a helical liquid is unconditionally stable with respect to single-particle backscattering [12], and can avoid the site with the Kondo singlet by penetrating into the bulk provided $K > 1/4$ [192, 193].

Because of the complexity of the many-body problems with either additional Rashba interaction, impurities or disorder, the above predictions have not yet been verified by simulations of microscopic models. Nevertheless, significant progress in the understanding of correlated helical edges has been made. The simplest scenario is the simultaneous breaking of time-reversal symmetry in the bulk *and* at the edge, as realized, for example, in the KMH model at large U/t (section 4.3). Because time-reversal symmetry is broken in the magnetic phase, a topologically trivial state without gapless edge states is expected. The evolution of the edge states across the magnetic bulk transition can only be studied in a model with an interacting bulk. Hence, the effective model of [125, 140] is insufficient. Instead, this problem has been studied in the framework of the KMH model by Wu *et al* [131] using cluster dynamical mean-field theory, and by Yu *et al* [132] using the variational cluster approach. Although these results do not fully capture the Luttinger liquid properties of the edge states, the results agree qualitatively with expectations. Figure 16 shows the single-particle spectral function for an armchair edge as obtained by Wu *et al* [131]. For the value $\lambda_{\text{SO}}/t = 0.2$ considered, the critical value for the bulk magnetic transition within their approximation is $U_c/t \approx 5.2$, which seems consistent with the observed opening of a gap in the edge states [131]. The low-energy model for the gapped edge states can be written as $H_{\text{HL}} - \tilde{g} m \sin(\sqrt{4\pi}\phi)$ (cf. (33)), where m is the bulk magnetization that, if nonzero, leads to a relevant perturbation for repulsive interactions [131]. A mean-field treatment with additional spin-wave fluctuations has been given by Lee [138].

To observe a topological insulator with Mott-insulating edges, time-reversal symmetry has to be broken at the edge. The observed tendency toward strong magnetic correlations follows already from the simple model (33), which predicts long-ranged but power-law transverse spin correlations for $K \ll 1$, see (34). The exponent K has been calculated numerically for different (spin-conserving) models [129, 140], and it was found that it can be substantially smaller than 1, see figures 14 and 17. However, as shown in figure 13, and in accordance with (34), true long-range order is absent even for very strong interactions [140]. Assuming that the edge states can be considered to be strictly one-dimensional, the absence of long-range order is implied by the Mermin-Wagner theorem, which forbids continuous symmetry breaking in one dimension. However, the continuous $U(1)$ spin symmetry can be reduced to a discrete Z_2 Ising symmetry in the presence of Rashba spin-orbit coupling in (4) or (6), or in more general models such as (9). In this case, umklapp processes of

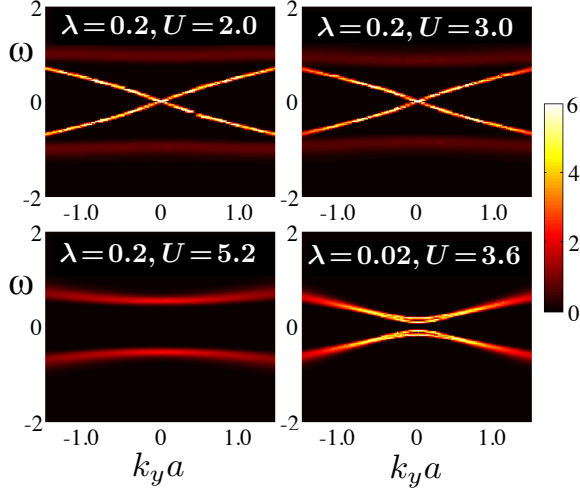


Figure 16. Single-particle spectral function of the KMH model on an armchair ribbon [131] with spin-orbit coupling $\lambda \equiv \lambda_{\text{SO}}$ and Hubbard interaction U . Results were obtained with the cluster dynamical mean-field theory. The top row corresponds to the quantum spin Hall phase, whereas the bottom row shows the spectrum in the magnetic (left) and the nonmagnetic insulator (right), respectively. (Reprinted with permission from [131]. Copyright 2012 by the American Physical Society).

the form (32) become possible, and give rise to Ising long-range magnetic order at $T = 0$ if $K < 1/2$ [78, 79, 138]. However, at $T > 0$, time-reversal symmetry will be restored by thermal fluctuations. This mechanism permits the existence of a topologically nontrivial quantum spin Hall insulator with gapped edge states and time-reversal symmetry, and causes the bulk-boundary correspondence to break down [119, 202, 203]. Temperature-dependent edge and bulk magnetism in a quantum spin Hall insulator has been discussed by Shitade *et al* [28]. The possibility of umklapp-driven magnetic order at the edge has been taken into account by Zheng *et al* [129] in their phase diagram of the KMH model. The latter, shown in figure 17, depicts a rather large region where $K < 1/2$, although the simulations were done for $\lambda_{\text{R}} = 0$. (The gap in the edge Green functions in [129] is a finite-size effect.) To determine K experimentally it may be useful to exploit the dependence of the single-particle gap induced by a magnetic field on the electron-electron interaction strength [195].

Based on the above arguments, and for models with conserved spin, the edge states are expected to become gapped exactly at the point where long-range magnetic order in the bulk breaks time-reversal symmetry and hence destroys the topological state. A slight complication is that the helical liquid is holographic, and hence exists only at the boundary of a two-dimensional system [78], whereas the absence of continuous symmetry breaking applies only to strictly one-dimensional systems. The two-dimensional bulk is not taken into account in the Luttinger model (33), but is included in the effective model with interactions only at the edge; no evidence for long-range

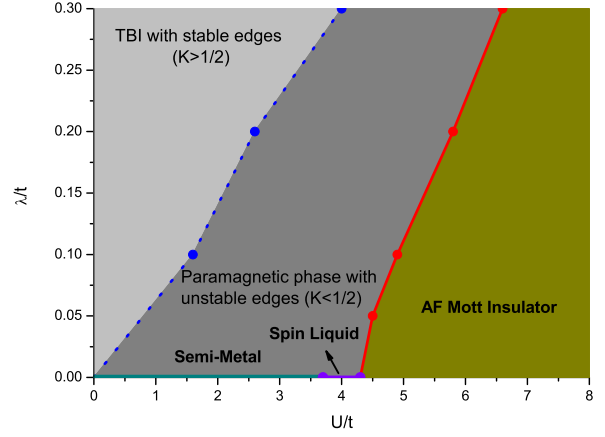


Figure 17. Phase diagram of the half-filled KMH model with spin-orbit coupling $\lambda \equiv \lambda_{\text{SO}}$ and Hubbard interaction U from quantum Monte Carlo simulations [129]. Also shown are regions where the Luttinger parameter $K < 1/2$ and $K > 1/2$, respectively. (Reprinted with permission from [129]. Copyright 2011 by the American Physical Society).

order has been found (see figure 13) [140]. For graphene edges, it has been argued that the Mermin-Wagner theorem is invalidated by the momentum dependence of electron-electron interactions, and numerical results are consistent with long-range magnetic order [199, 200].

The difficulties associated with capturing large length scales (cf. figure 13) and quantum fluctuations, as well as with the unambiguous detection of topological states, have led to several claims for the existence of edge Mott insulators (or edge superconductors) in systems with conserved spin. Paramagnetic, inhomogeneous slave-rotor calculations for the KMH and the BHZH model suggest the existence of a paramagnetic edge-Mott state for large values of λ_{SO} [94]. Similar conclusions have been drawn based on variational Monte Carlo simulations of the KMH model [130]. Finally, a symmetry-breaking superconducting state has been reported for the KMH model with attractive interactions [205] based on a mean-field calculation. In two dimensions, the slave-rotor result [94] is known to be unstable with respect to gauge fluctuations [87]. A similar but stable phase (a topological Mott insulator) has been predicted based on slave-boson calculations [135]. The variational Monte Carlo results for the spin and charge Drude weights [130] have rather large error bars, and the authors interpret them either as a transition or a crossover. The latter possibility agrees with other numerical work [125, 131, 140], see discussion below.

The existence of a superconducting edge state can be excluded by exploiting the exact particle-hole symmetry of the KMH Hamiltonian, and the canonical transformation $c_{i\uparrow}^\dagger \mapsto (-1)^i c_{i\downarrow}$, with $(-1)^i = \pm 1$ depending on the sublattice. Similar to the Hubbard model, this transformation exchanges the role of spin- z and charge operators in the Hamiltonian, and flips the sign of the Hubbard term [206]. The dominant transverse spin

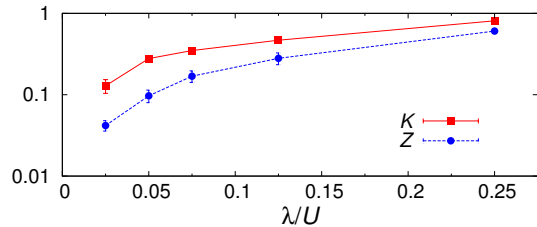


Figure 18. Luttinger liquid parameter K and spectral weight of long-wavelength charge excitations Z from quantum Monte Carlo simulations of an effective model for helical edge states. (Reprinted with permission from [140]. Copyright 2012 by the American Physical Society).

correlations observed in the repulsive model translate into dominant pairing correlations $P(r)$ in the attractive model. However, all correlation functions decay with a power law, as can be explicitly confirmed by quantum Monte Carlo simulations for the attractive case [207]. The symmetry breaking observed in [205] at the mean-field level hence has the same origin as the long-range magnetic order in repulsive model, namely a logarithmically divergent susceptibility [138].

Although no gap is opened in quantum spin Hall insulators with conserved spin, strong interactions lead to important modifications of the edge states. Apart from a renormalization of the velocity v with increasing U/λ_{SO} that follows from the low-energy model (33), see figure 14, numerical studies indicate a suppression of charge transport, visible for example in the dynamical charge structure factor at long wavelengths and low energies in figure 15(b), or in the Drude weight [130], with a simultaneous enhancement of spectral weight for transverse spin excitations [125, 130, 140]. Similarly, the spectral weight of the edge states in the single-particle spectrum is diminished by strong interactions [125, 131, 140].

The Drude weight, D , can be related to the spectral weight, Z , of the linear mode in the dynamical charge structure factor via $D = Zv$ (v being the velocity); Z can be measured in quantum Monte Carlo simulations [140], and results are shown in figure 18. On the other hand, for a Luttinger liquid described by (33), the Drude weight is given by $D = Kv$ [140], so that the apparent difference between Z and K in figure 18 indicates that the model (33) is incomplete. While $Z = K$ in the noninteracting limit, the Drude weight is significantly smaller than predicted theoretically (i.e., smaller than $D = Kv$) for nonzero interactions. The discrepancy has been attributed to inelastic spin-flip scattering mediated by the pronounced magnetic fluctuations that exist for $K \ll 1$, and to scattering processes that involve bulk states [140]. Whereas bulk effects are expected if the interaction U becomes comparable or larger than the bulk band gap, the numerical results suggest that deviations occur even for rather weak interactions [140].

6. Topological invariants of correlated systems

The discovery of the remarkable relation between the quantized Hall conductivity and the first Chern number in the context of the quantum Hall effect [4–6] has played a key role for the understanding of topological phases of matter. In section 3, it has been shown that a topological invariant can also be defined for quantum spin Hall insulators, and that the latter is—in the simplest case—determined by the Chern number difference of two quantum Hall states with opposite Hall conductivities [86]. Reviews of topological invariants with a focus on noninteracting systems can be found in [14, 26, 50]. Here the emphasis is on the calculation of topological invariants for correlated systems by means of numerical methods. More general discussions can be found, for example, in [26, 208].

Whereas the direct calculation of the topological invariant of interacting systems can be rather difficult, its value can in some cases be inferred indirectly either via the bulk-boundary correspondence, or based on an adiabatic connection to a noninteracting system.

Because time-reversal symmetry protects topological insulators against weak interactions, the bulk-boundary correspondence can in principle be used to determine whether or not a topological state survives upon switching on electron-electron interactions. However, this approach, followed for example in [98, 131, 132], faces a number of difficulties. In addition to the inherent difficulty of obtaining numerical results on large enough systems with open boundaries to demonstrate the existence of gapless excitations, correlation effects and electron tunnelling between edges can gap out the edge states despite the existence of topological order in the bulk (see section 5.2). Although gapped edge states can be reconciled with a nonzero topological invariant theoretically [119, 202, 203], a distinction of topological and trivial states based on edge states alone will be challenging in actual numerical calculations for strongly correlated systems. Nevertheless, the bulk-boundary correspondence is a valuable theoretical concept. For example, it has been used to formulate criteria for the stability [41, 124] and the experimental identification [179] of fractional topological insulators. The existence of gapless edge states can also be inferred from the theory of symmetry-protected topological states [44–49].

A topological phase may also be identified by exploiting an adiabatic connection to a noninteracting state (for which the invariant can easily be calculated). For example, as discussed in section 4.2, the KMH model with $\lambda_{\text{R}} = 0$ describes a quantum spin Hall state for $U = 0$ and $\lambda_{\text{SO}} \neq 0$. For small to intermediate values of U/t , the system remains fully gapped and time-reversal invariant, and can be adiabatically tuned (via U/t) into the noninteracting quantum spin Hall state without closing the band gap, see Fig. 6. This argument establishes the topological character of the state at $U > 0$. As

emphasized in section 4.5, no such adiabatic connection to a noninteracting state exists, for example, in the case of fractional topological insulators or topological Mott insulators. Finally, even using exact numerical methods, it is not always possible to decide if an excitation gap closes or not across a transition [126].

Given the limitations of these indirect probes for topological states, it is important to be able to directly calculate the topological invariant. For spin-conserved quantum spin Hall insulators, it is sufficient to determine the Chern number for one spin sector. Because the Chern number is related to the quantized Hall conductivity, it can in principle be obtained without approximations from the Kubo formula [113, 114]. The Z_2 invariant then follows from (15). Nevertheless, for correlated electron systems, even the calculation of the conductivity can be quite demanding. When spin is not conserved, the separation into two spin sectors is obviously no longer possible, and other concepts such as the spin Chern number are required. In particular, even an exact calculation of the Hall conductivity via the Kubo formula may be insufficient because σ_{xy}^s is no longer quantized [86].

Considering first the integer, spin-conserved case, (13) and (14) are not applicable to interacting systems, because they rely on a representation in terms of Bloch states. Instead, the Chern number in the presence of interactions and/or disorder can be calculated from [113]

$$C = \int \int_0^{2\pi} \frac{d\phi_x d\phi_y}{2\pi i} \left[\left\langle \frac{\partial \Psi_0}{\partial \phi_y} \middle| \frac{\partial \Psi_0}{\partial \phi_x} \right\rangle - (y \leftrightarrow x) \right]. \quad (35)$$

Compared to (13), the Bloch states $|u_m\rangle$ are replaced by the many-body ground state $|\Psi_0\rangle$, and the momenta k_x, k_y are replaced by phase parameters ϕ_x, ϕ_y describing general boundary conditions $\Psi_0(\dots, \{x_i + L_x, y_i\}, \dots) = e^{i\phi_x} \Psi_0(\dots, \{x_i, y_i\}, \dots)$ (and similar for the y direction) [113]. On a torus geometry, the phase shifts ϕ_x, ϕ_y can be related to magnetic fluxes [114]. Assuming the existence of a bulk energy gap and a unique, nondegenerate ground state, C as defined by (35) is an integer Chern number directly related to the Hall conductivity [113]. An alternative representation is given by [113, 114]

$$C = \int \int_0^{2\pi} \frac{d\phi_x d\phi_y}{2\pi i} \times \sum_{n>0} \frac{\langle \Psi_0 | \frac{\partial H}{\partial \phi_y} | \Psi_n \rangle \langle \Psi_n | \frac{\partial H}{\partial \phi_x} | \Psi_0 \rangle - (y \leftrightarrow x)}{(E_n - E_0)^2}. \quad (36)$$

The derivatives of the Hamiltonian are numerically easier to evaluate than derivatives of the wave functions [114], and (36) reveals the relation to the Kubo formula [114]. For simplicity, the zero-temperature limit has been taken. At finite temperatures, the Hall and spin Hall conductivities are in general not exactly quantized, see for example [97, 209].

Equations (35) and (36) can be extended to the case of a fractional quantum Hall state with a d -dimensional

ground-state manifold $\{|\Psi_K\rangle\}$, $K = 1, \dots, d$. The Chern number reads [113]

$$C = \frac{1}{d} \int \int_0^{2\pi} \frac{d\phi_x d\phi_y}{2\pi i} \times \sum_{K=1}^d \left[\left\langle \frac{\partial \Psi_K}{\partial \phi_y} \middle| \frac{\partial \Psi_K}{\partial \phi_x} \right\rangle - \left\langle \frac{\partial \Psi_K}{\partial \phi_x} \middle| \frac{\partial \Psi_K}{\partial \phi_y} \right\rangle \right]. \quad (37)$$

The corresponding generalization of (36) to the fractional case can be found, for example, in [210]. Equations (35)–(37) are particularly useful in combination with exact diagonalization methods, and recent applications in the context of correlated Chern insulators include [40, 90, 92, 210]. Twisted boundary conditions can also be used in combination with quantum Monte Carlo simulations [90].

A generalization for integer quantum spin Hall insulators without spin conservation is based on the Chern number matrix [86, 117]

$$C^{\sigma\sigma'} = \int \int_0^{2\pi} \frac{d\phi_x^\sigma d\phi_y^{\sigma'}}{2\pi i} \times \left[\left\langle \frac{\partial \Psi_0}{\partial \phi_y^{\sigma'}} \middle| \frac{\partial \Psi_0}{\partial \phi_x^\sigma} \right\rangle - \left\langle \frac{\partial \Psi_0}{\partial \phi_x^\sigma} \middle| \frac{\partial \Psi_0}{\partial \phi_y^{\sigma'}} \right\rangle \right], \quad (38)$$

with spin-dependent boundary twists $\phi_x^\sigma, \phi_y^{\sigma'}$. If spin is conserved, $C^{\uparrow\downarrow} = C^{\downarrow\uparrow} = 0$ whereas $C^{\uparrow\uparrow} = C^{\downarrow\downarrow} = \pm 1$. Sheng *et al* [86] defined a total charge Chern number $C^c = \sum_{\sigma\sigma'} C^{\sigma\sigma'}$ and a total spin Chern number $C^s = \sum_{\sigma\sigma'} \sigma C^{\sigma\sigma'}$. In contrast to σ_{xy}^s , which is only quantized if spin is conserved (in this case, the calculation of σ_{xy}^s and C^s are completely equivalent, see section 3), the spin Chern number C^s as defined in [86] remains quantized throughout the topological phase of the KM model with $\lambda_R \neq 0$ and/or disorder [86]. Whereas Sheng *et al* [86] suggest that (38) permits one to distinguish two different quantum spin Hall phases (with the sign of σ_{xy}^s depending on the sign of the spin-orbit coupling), Fu and Kane [119] as well as Fukui and Hatsugai [211] argue that this distinction is merely a boundary effect, and that the state is fully characterized by a Z_2 index $\nu = 1$. The flux insertion related to the twisted boundary conditions can cause a spurious closing of the band gap on small systems [211, 212]. Although (35) and (39) are equivalent for the spin-conserved case, it is not clear if the above definition of the spin Chern number can also be applied (and remains quantized) to fractional topological insulators without spin conservation [165].

Equation (38) provides a rather general way to calculate the Z_2 index in correlated topological phases with time-reversal symmetry. However, its numerical evaluation can be quite involved or even technically impossible in the context of numerical approaches based on quantum Monte Carlo or quantum cluster methods. Consequently, a lot of effort has been devoted to developing simplified ways of calculating topological invariants.

The starting point for one of the most fruitful recent developments is to express the Chern number in terms of the

single-particle Green function [116, 203, 209, 213–215],

$$C = \frac{\epsilon^{\mu\nu\rho}}{6} \int dk_0 \int \frac{dk_x dk_y}{(2\pi)^2} \quad (39)$$

$$\times \text{tr} \left[G \partial_\mu G^{-1} G \partial_\nu G^{-1} G \partial_\rho G^{-1} \right],$$

with $k_0 = \omega$ (and ω real), $\mathbf{k} = (k_x, k_y)$, and $\partial_\mu \equiv \partial/\partial k_\mu$ etc. $G = G(i\omega, \mathbf{k})$ is the frequency and momentum-dependent single-particle Green function (in general a matrix in spin and orbital space), and G^{-1} its matrix inverse [203]. The trace is over the matrix indices of G and G^{-1} , and a summation over μ, ν , and ρ is implied. Equation (39) can be applied to spin-conserving quantum spin Hall systems by calculating C in each spin sector, see for example [97, 101]. In this context, stochastic integration methods have been employed to sample the strongly varying integrands [216], and an algorithm that preserves gauge invariance and the quantization of the Chern number even on a discretized Brillouin zone has been given [217]. A simplification of (39), valid within the local approximation of dynamical mean-field theory, has been used to calculate σ_{xy}^s for the BHZH model [97], see figure 8. The Z_2 invariant of general, time-reversal invariant insulators can also be expressed in terms of the Green function; it is related to the electromagnetic polarization, and involves a five-dimensional integral [215].

Equation (39) can in principle be used directly to calculate the Chern number. Moreover, the formulation in terms of the single-particle Green function provides valuable insights into the bulk-boundary correspondence and interaction effects by analyzing the properties of G itself [116, 203, 218]. Most importantly, (39) implies that the Chern number can only change if a singularity appears in either G or G^{-1} [203, 218]. Considering first a noninteracting system, the relation $G(i\omega, \mathbf{k}) = [i\omega - H(\mathbf{k})]^{-1}$ reveals that, for ω on the real axis, poles can only occur at $\omega = 0$, where they are related to zero eigenvalues of H and hence to zero-energy states. The change of C in this case is hence related to either a closing of the bulk band gap, or to an interface with a topologically different system where the zero-energy states correspond to edge states. In this way, the Green function can be used to derive the bulk-boundary correspondence principle [218].

In interacting systems, poles in the self-energy and hence in G^{-1} provide another mechanism for a change of the Chern number [133, 203], see (39). However, as pointed out in [203, 218], such *Green function zeros* are in general not related to a gap closing or to the existence of edge states. Consequently, the bulk-boundary correspondence can break down in the presence of interactions [203, 218]. Although intuitive, this picture based on the single-particle Green function may not capture interaction-generated collective excitations [203], such as gapless spinon excitations in a topological Mott insulator [36].

Whereas (39) is exact for noninteracting systems, its physical meaning is not yet fully understood in the

interacting case. As discussed in [26, 203], for interacting systems, (39) relies on an adiabatic connection between the interacting state and a noninteracting, topological band insulator. It is therefore in general not applicable to interaction-driven states such as topological Mott insulators and fractional topological insulators. Although (39) remains a quantized, topological quantity even in the presence of interactions [203], its relation to physical observables such as σ_{xy}^s for general interacting states is an interesting open question [26, 203, 218, 219]. On the other hand, (39) can be extended to disordered systems by replacing the physical momenta with phases representing twisted boundary conditions [26]. The Green function has also been used to study topological superconductors [220, 221], and correlated topological states in one [222] and three dimensions [223].

The multiple integrals, and the required knowledge of the Green function and its derivative, make the numerical evaluation of (39) rather difficult. Starting from (39), further simplifications have been achieved by Wang and Zhang [224] and by Wang *et al* [225], and the single-particle Green function again plays a key role. Wang and Zhang [224] showed that given an adiabatic connection to a noninteracting state (see also [26]), the topological invariant can be obtained from the Green function at $\omega = 0$ only [224], thereby simplifying practical calculations significantly. As shown in [224], the Chern number can be written in the form (13), with the Berry flux defined over the space of eigenvalues of the zero-frequency Green function. A related, physically more intuitive concept is the so-called *topological Hamiltonian* defined as $\tilde{h}(\mathbf{k}) = -G^{-1}(0, \mathbf{k}) = h_0(\mathbf{k}) + \Sigma(0, \mathbf{k})$ [208], where $h_0(\mathbf{k})$ is the noninteracting part of a many-body Hamiltonian, and $\Sigma(0, \mathbf{k})$ is the zero-frequency part of the self-energy. Remarkably, provided there is an adiabatic connection to a noninteracting system, the topological Hamiltonian captures the topological invariant of the full, interacting problem [224]; see also [26, 208]. It therefore provides a highly nontrivial extension of the fact that for a noninteracting system, where $-G^{-1}(0, \mathbf{k}) = H(\mathbf{k})$, the Green function inherits the symmetries (time-reversal, particle-hole, and chiral symmetry) of the Hamiltonian, and can hence be used for a topological classification [218]. An illuminating discussion of why the zero-frequency self-energy is sufficient to calculate the topological invariant can be found in [208]. For practical applications, the power of the concept of the topological Hamiltonian is related to the possibility of calculating the Chern number by any method that is applicable to noninteracting systems. For example, given inversion symmetry, the Green function has to be determined only at the four time-reversal invariant momenta [225]. This method has been applied to the KMH model [133] and the BHZH model [100], and is quite similar in spirit to the work of Fu and Kane [8], in which the eigenvalues of the parity operator at the time-

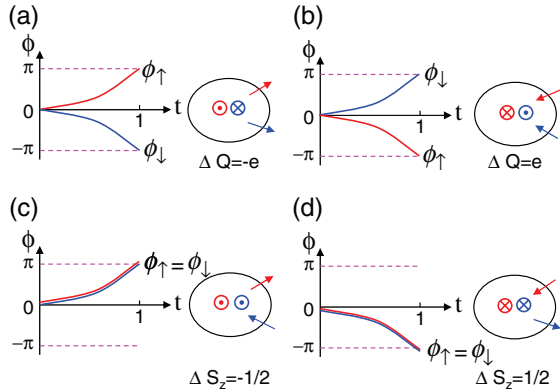


Figure 19. The four possible adiabatic processes $\phi_{\uparrow}(t)$, $\phi_{\downarrow}(t)$ for inserting a π flux into a quantum spin Hall insulator [228]. Considering a closed loop around the flux, Faraday’s law implies the existence of charge fluxons with charge $\pm e$ and spin 0, and spin fluxons with charge 0 and spin $\pm 1/2$. (Reprinted with permission from [228]. Copyright 2008 by the American Physical Society).

reversal invariant points in the Brillouin zone determine the topological invariant.

In addition to this rather general approach, several other simplifications have been proposed and used in combination with numerical methods. The calculation of topological invariants becomes even simpler if the self-energy is local, i.e., independent of \mathbf{k} . This approximation underlies the dynamical mean-field theory, and is expected to yield quite accurate results in high dimensions [226]. Wang *et al* [227] showed that a local self-energy that is diagonal in orbital space permits one to write the Chern number as a product of the *frequency-domain winding number* and a Chern number of a mean-field Hamiltonian. The former is related to fluctuation-driven topological phase transitions, whereas the latter captures band structure effects. This idea has been successfully applied to the KMH model [133]. For local self-energies that are not diagonal in orbital space, a simplification can be achieved using a pole expansion of the self-energy, and leads to an effective, noninteracting Hamiltonian whose topological invariant can be shown to be the same as that of the original, correlated model [216]. Applications of this method can be found in [98, 133, 216]. Interestingly, these calculations predict interaction-driven transitions to topological phases that are not captured by mean-field theory and hence related to quantum fluctuations [98, 133]. A drawback for applications to two-dimensional systems is the complete neglect of spatial correlations.

Topological insulators can also be identified by their response to topological defects such as π fluxes [154, 228], twisted boundary conditions [229], dislocations [93], vacancies [230], or disclinations [231]. Such defects, near which the topological properties are perturbed compared to the rest of the system, typically give rise to new, low-energy

excitations with well-defined quantum numbers. Similar to the metallic edge states arising from open boundary conditions, the existence of these states is protected by time-reversal symmetry. They also have a close conceptual relation to the familiar soliton excitations in polyacetylene first proposed by Su *et al* [232]. For numerical methods, π fluxes are of particular interest as they can be easily implemented, and will be the focus here.

The existence of low-energy excitations as a result of a π flux becomes quite apparent from the flux insertion argument by Qi and Zhang [228]; see also [14]. Consider a disk-shaped, noninteracting quantum spin Hall insulator that conserves spin [228]. Through a hole at the centre, a magnetic flux of magnitude $hc/2e$ (equal to π in units where $\hbar = c = e = 1$) is inserted adiabatically. This insertion can be described by the time-dependent fluxes $\phi_{\uparrow}(t)$, $\phi_{\downarrow}(t)$, with $\phi_{\sigma}(t=0) = 0$ and $\phi_{\sigma}(t=1) = \pm\pi$. In total, there are four different possibilities to switch on the fluxes that differ by the signs of the fluxes $\phi_{\uparrow}(t)$ and $\phi_{\downarrow}(t)$, as shown in figure 19. Importantly, because the resulting Berry phases $e^{i\pi} = e^{-i\pi} = -1$, all four choices lead to the same final state [228]. Considering a loop around the flux tube, Faraday’s law states that the flux gives rise to a tangential electric field, which for a quantum spin Hall insulator in turn causes a flow of charge perpendicular to the loop. The four different processes give rise to a doublet of states with charge $Q = \pm e$ and spin $S^z = 0$ (the so-called *charge fluxons* [154], figure 19(a) and (b)), and a pair of states with charge $Q = 0$ and spin $S^z = \pm 1/2$ (*spin fluxons* [154], figure 19(c) and (d)). Given time-reversal and particle-hole symmetry, these states can be shown to lie in the middle of the band gap [154, 228]. Moreover, they are exponentially localized near the π flux, and the two spin fluxon states form a Kramers doublet related by time reversal, just like the two states of a spin 1/2. The whole argument can also be generalized to systems with only a Z_2 spin symmetry [228].

Fluxon states as a response to a π flux provide an alternative way to define the Z_2 topological invariant, and were suggested to be a useful tool to study correlated topological states in combination with numerical methods [154, 228]. In particular, there is no need to study systems with open boundaries, or to perform high-dimensional integrals over Green functions. On periodic lattices, π fluxes can be inserted in pairs, and are implemented in terms of Berry phase factors for hopping processes that cross the *string* or *branch cut* that connects two fluxes [127, 228, 229]. A first study in this direction was recently carried out based on exact quantum Monte Carlo simulations of the KMH model [127]. In that work, it was established that the spin fluxon states can be identified from a characteristic Curie law (given by $N_{\pi}/k_B T$ for N_{π} fluxes) in the temperature-dependent magnetic susceptibility. This Curie law is related to the low-energy spin fluxon doublet (in the presence of repulsive

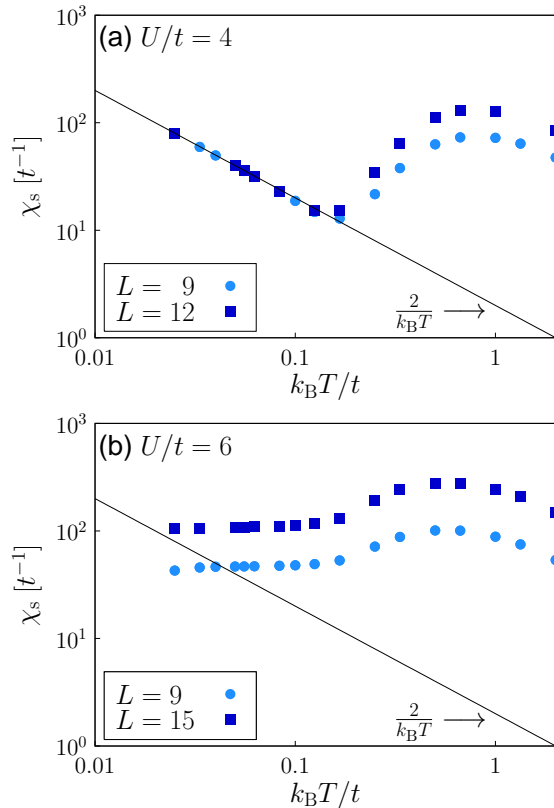


Figure 20. Magnetic susceptibility of the KMH model with one pair of π fluxes from quantum Monte Carlo simulations on $L \times L$ lattices. (a) In the quantum spin Hall phase, midgap spin fluxon states give rise to a Curie law at low temperatures. In contrast, such a Curie law is absent in the results for the magnetic insulating state shown in (b). Data taken from [127].

electronic interactions, charge fluxon states become gapped [154, 228]). As illustrated in figure 20, the presence or absence of a Curie law at low temperatures provides a clear distinction between a correlated quantum spin Hall state and an antiferromagnet with spontaneously broken time-reversal symmetry [127]. The presence of localized spin fluxon excitations can also be visualized by means of the lattice-site dependent spin excitation spectrum [127]. Based on the flux insertion argument (figure 19), a generalization to fractional topological insulators seems possible.

Finally, quantum entanglement [44] has in recent years emerged as one of the most useful tools to detect topological order in numerical calculations, most notably in the framework of the density matrix renormalization group and related approaches [233]. The *entanglement entropy* [234–236] is calculated as the partial trace over the density matrix of the ground state and provides a measure for the quantum correlations between different parts of the quantum system under consideration. It directly reveals the presence of excitations with exotic quantum numbers and can be used to identify, for example, quantum spin liquids [237, 238] and the exotic QSH* phase of the SI model [102]. Even more information is contained

in the *entanglement spectrum* [239], corresponding to the spectrum of the reduced density matrix. In the context of topological insulators, it has been shown that topological phases possess protected gapless modes in their entanglement spectrum, which remain gapless even if the physical edge states are gapped out by interaction effects or perturbations that break time-reversal symmetry [240, 241]; for more details see [76, 107] and references therein. Whereas the two-dimensional setting of quantum spin Hall insulators is typically difficult to study with the density matrix renormalization group method, important progress has been made using tensor networks, and a suitable ansatz for fractional topological insulators has been proposed in [181]. For recent advances in the application to quantum Hall states see [242].

7. Conclusions and outlook

Despite their rather short history, time-reversal invariant topological insulators have already evolved into a multifaceted research field driven by interests ranging from future technological applications of the quantum spin Hall effect to the intricate physics of interaction-driven topological order. This review has aimed at providing an overview of the fascinating topic of electronic correlation effects, which on their own have been at the focus of attention in the condensed matter community for decades. Similar to the fractional quantum Hall effect, the combination of electron-electron interactions and topological aspects in strongly-correlated topological insulators provides an ideal setting to explore beautiful new physics.

Among the two-dimensional systems discussed here, the currently best understood correlated topological insulators are those with strong, intrinsic spin-orbit coupling that gives rise to a topological band insulator in the absence of electronic correlations. If spin is conserved, such states have close conceptual relations to the integer quantum Hall effect. The impact of electronic interactions can in many cases be explored by means of sophisticated numerical methods. Because time-reversal symmetry is at the heart of topological insulators, magnetic correlations induced by strong electron-electron interactions play a crucial role. For several of the available theoretical models, it is known that an extended topological insulator phase exists up to rather strong electronic interactions, and is adiabatically connected to a topological band insulator. At even stronger interactions, time-reversal symmetry can be spontaneously broken by the onset of long-range magnetic order. Generically, such a transition destroys the topological state but under special conditions, antiferromagnetic topological insulators with robust edge states exist.

Correlation effects also play an important role for the helical edge states. Time-reversal symmetry provides protection against single-particle backscattering processes, but two-particle backscattering can give rise to long-range

magnetic order at the edge, and to a breakdown of the bulk-boundary correspondence. However, whereas the relevant Luttinger parameter has been shown to become small enough for such a transition to occur, the necessary umklapp scattering is not allowed if spin is conserved. In the absence of magnetic impurities, the edges therefore retain their metallic character even for strong interactions. Helical edge states are also remarkably different from ordinary one-dimensional liquids concerning their stability with respect to magnetic impurities or disorder.

Topological states that are not adiabatically connected to band insulators have been explored less thoroughly. Examples include topological Mott insulators, in which the topological state is generated from electronic correlations rather than from spin-orbit coupling, and fractional topological insulators that can, in the simplest case, be constructed by combining two fractional quantum Hall states in a time-reversal invariant way. In these cases, the resulting many-body state cannot be understood in the noninteracting limit, and intriguing phenomena such as quasiparticles with fractional charge and statistics appear. Moreover, while Rashba spin-orbit coupling—violating the conservation of total spin—is often considered as an experimental nuisance, theoretical results suggest that it may actually lead to exciting and not yet fully explored new physics. Topological Mott insulators and fractional topological insulators, as well as the general class of topologically ordered states with time-reversal symmetry, have so far been studied mostly using mean-field or topological field theory, and pose challenging problems such as finding suitable ways to determine whether or not a given state is topological. The identification and comprehensive numerical investigation of microscopic models is one of the future goals. An important recent development is the use of quantum entanglement and local unitary transformations to study and classify phases with topological order as well as symmetry-protected topological states such as topological insulators. Finally, the current search for experimental realizations, for example in cold-atom systems and transition-metal oxide heterostructures, will hopefully soon lead to a fruitful interplay of theory and experiment.

The authors are grateful to M. Bercx, B. Béri, J. Budich, N. Cooper, M. Daghofer, V. Gurarie, M. Kharitonov, T. Lang, M. Laubach, A. Liebsch, Z. Meng, J. Moore, A. Muramatsu, S. Rachel, M. Schmidt, R. Thomale, B. Trauzettel, C. Varney, S. Wessel, and C. Xu for valuable discussions. Financial support from the DFG grants As 120/4-3 and Ho 4489/2-1 is gratefully acknowledged.

References

- [1] V. L. Ginzburg and L. D. Landau, *Zh. Eksp. Teor. Fiz.* **20**, 1064 (1950).
- [2] K. v. Klitzing, G. Dorda, and M. Pepper, *Phys. Rev. Lett.* **45**, 494 (1980).
- [3] C. Nayak, S. H. Simon, A. Stern, M. Freedman, and S. Das Sarma, *Rev. Mod. Phys.* **80**, 1083 (2008).
- [4] D. J. Thouless, M. Kohmoto, M. P. Nightingale, and M. den Nijs, *Phys. Rev. Lett.* **49**, 405 (1982).
- [5] J. E. Avron, R. Seiler, and B. Simon, *Phys. Rev. Lett.* **51**, 51 (1983).
- [6] M. Kohmoto, *Annals of Physics* **160**, 343 (1985).
- [7] B. I. Halperin, *Phys. Rev. B* **25**, 2185 (1982).
- [8] L. Fu and C. L. Kane, *Phys. Rev. B* **76**, 045302 (2007).
- [9] F. D. M. Haldane, *Phys. Rev. Lett.* **61**, 2015 (1988).
- [10] J. E. Moore and L. Balents, *Phys. Rev. B* **75**, 121306 (2007).
- [11] C. L. Kane and E. J. Mele, *Phys. Rev. Lett.* **95**, 146802 (2005).
- [12] C. L. Kane and E. J. Mele, *Phys. Rev. Lett.* **95**, 226801 (2005).
- [13] L. Fu, C. L. Kane, and E. J. Mele, *Phys. Rev. Lett.* **98**, 106803 (2007).
- [14] X.-L. Qi and S.-C. Zhang, *Rev. Mod. Phys.* **83**, 1057 (2011).
- [15] H. Min, J. E. Hill, N. A. Sinitsyn, B. R. Sahu, L. Kleinman, and A. H. MacDonald, *Phys. Rev. B* **74**, 165310 (2006).
- [16] C.-C. Liu, W. Feng, and Y. Yao, *Phys. Rev. Lett.* **107**, 076802 (2011).
- [17] P. Vogt, P. De Padova, C. Quaresima, J. Avila, E. Frantzeskakis, M. C. Asensio, A. Resta, B. Ealet, and G. Le Lay, *Phys. Rev. Lett.* **108**, 155501 (2012).
- [18] A. Fleurence, R. Friedlein, T. Ozaki, H. Kawai, Y. Wang, and Y. Yamada-Takamura, *Phys. Rev. Lett.* **108**, 245501 (2012).
- [19] L. Chen, C.-C. Liu, B. Feng, X. He, P. Cheng, Z. Ding, S. Meng, Y. Yao, and K. Wu, *Phys. Rev. Lett.* **109**, 056804 (2012).
- [20] M. König, S. Wiedmann, C. Brüne, A. Roth, H. Buhmann, L. W. Molenkamp, X.-L. Qi, and S.-C. Zhang, *Science* **318**, 766 (2007).
- [21] A. Roth, C. Brüne, H. Buhmann, L. W. Molenkamp, J. Maciejko, X.-L. Qi, and S.-C. Zhang, *Science* **325**, 294 (2009).
- [22] C. Brüne, A. Roth, H. Buhmann, E. M. Hankiewicz, L. W. Molenkamp, J. Maciejko, X.-L. Qi, and S.-C. Zhang, *Nat. Phys.* **8**, 486 (2012).
- [23] B. A. Bernevig, T. L. Hughes, and S. Zhang, *Science* **314**, 1757 (2006).
- [24] A. P. Schnyder, S. Ryu, A. Furusaki, and A. W. W. Ludwig, *Phys. Rev. B* **78**, 195125 (2008).
- [25] A. Kitaev, *AIP Conf. Proc.* **1134**, 22 (2009).
- [26] J. C. Budich and B. Trauzettel, *physica status solidi (RRL)* **7**, 109 (2013).
- [27] R.-J. Slager, A. Mesaros, V. Juricic, and J. Zaanen, *Nat. Phys.* **9**, 98 (2013).
- [28] A. Shitade, H. Katsura, J. Kunes, X.-L. Qi, S.-C. Zhang, and N. Nagaosa, *Phys. Rev. Lett.* **102**, 256403 (2009).
- [29] J. Reuther, R. Thomale, and S. Trebst, *Phys. Rev. B* **84**, 100406 (2011).
- [30] J. Chaloupka, G. Jackeli, and G. Khaliullin, *Phys. Rev. Lett.* **105**, 027204 (2010).
- [31] J. Reuther, R. Thomale, and S. Rachel, *Phys. Rev. B* **86**, 155127 (2012).
- [32] M. Kargarian, A. Langari, and G. A. Fiete, *Phys. Rev. B* **86**, 205124 (2012).
- [33] S. Okamoto, *Phys. Rev. Lett.* **110**, 066403 (2013).
- [34] L. Balents, *Nature* **464**, 199 (2010).
- [35] S. Raghu, X. Qi, C. Honerkamp, and S. Zhang, *Phys. Rev. Lett.* **100**, 156401 (2008).
- [36] D. Pesin and L. Balents, *Nat. Phys.* **6**, 376 (2010).
- [37] B. J. Kim, H. Jin, S. J. Moon, J.-Y. Kim, B.-G. Park, C. S. Leem, J. Yu, T. W. Noh, C. Kim, S.-J. Oh, J.-H. Park, V. Durairaj, G. Cao, and E. Rotenberg, *Phys. Rev. Lett.* **101**, 076402 (2008).
- [38] B. J. Kim, H. Ohsumi, T. Komesu, S. Sakai, T. Morita, H. Takagi, and T. Arima, *Science* **323**, 1329 (2009).
- [39] D. N. Sheng, Z.-C. Gu, K. Sun, and L. Sheng, *Nat. Commun.* **2**, 389 (2011).
- [40] J. W. F. Venderbos, S. Kourtis, J. van den Brink, and M. Daghofer, *Phys. Rev. Lett.* **108**, 126405 (2012).
- [41] M. Levin and A. Stern, *Phys. Rev. Lett.* **103**, 196803 (2009).

- [42] Y.-M. Lu and A. Vishwanath, *Phys. Rev. B* **86**, 125119 (2012).
- [43] X.-G. Wen, *Quantum Field Theory of Many-body Systems: From the Origin of Sound to an Origin of Light and Electrons* (Oxford University Press, Oxford, 2004).
- [44] X. Chen, Z.-C. Gu, and X.-G. Wen, *Phys. Rev. B* **82**, 155138 (2010).
- [45] X. Chen, Z.-X. Liu, and X.-G. Wen, *Phys. Rev. B* **84**, 235141 (2011).
- [46] X. Chen, Z.-C. Gu, Z.-X. Liu, and X.-G. Wen, arXiv:1106.4772 (2011).
- [47] X. Chen, Z.-C. Gu, Z.-X. Liu, and X.-G. Wen, *Science* **21**, 1604 (2012).
- [48] C. Xu, arXiv:1209.4399 (2012).
- [49] J. Oon, G. Y. Cho, and C. Xu, arXiv:1212.1726 (2012).
- [50] M. Z. Hasan and C. L. Kane, *Rev. Mod. Phys.* **82**, 3045 (2010).
- [51] M. Z. Hasan and J. E. Moore, *Annu. Rev. Cond. Mat. Phys.* **2**, 55 (2011).
- [52] S. Wolgast, C. Kurdak, K. Sun, J. W. Allen, D.-J. Kim, and Z. Fisk, arXiv:1211.5104 (2012).
- [53] J. Botimer, D. J. Kim, S. Thomas, T. Grant, Z. Fisk, and J. Xia, arXiv:1211.6769 (2012).
- [54] X. Zhang, H. Zhang, J. Wang, C. Felser, and S.-C. Zhang, *Science* **335**, 1464 (2012).
- [55] D. Xiao, W. Zhu, Y. Ran, N. Nagaosa, and S. Okamoto, *Nat. Commun.* **2**, 596 (2011).
- [56] X. Hu, A. Rüegg, and G. A. Fiete, *Phys. Rev. B* **86**, 235141 (2012).
- [57] K.-Y. Yang, W. Zhu, D. Xiao, S. Okamoto, Z. Wang, and Y. Ran, *Phys. Rev. B* **84**, 201104 (2011).
- [58] A. Rüegg and G. A. Fiete, *Phys. Rev. B* **84**, 201103 (2011).
- [59] A. Rüegg, C. Mitra, A. A. Demkov, and G. A. Fiete, *Phys. Rev. B* **85**, 245131 (2012).
- [60] F. Wang and Y. Ran, *Phys. Rev. B* **84**, 241103 (2011).
- [61] R. Nandkishore and L. Levitov, *Phys. Rev. B* **82**, 115124 (2010).
- [62] F. Zhang, J. Jung, G. A. Fiete, Q. Niu, and A. H. MacDonald, *Phys. Rev. Lett.* **106**, 156801 (2011).
- [63] C. Weeks, J. Hu, J. Alicea, M. Franz, and R. Wu, *Phys. Rev. X* **1**, 021001 (2011).
- [64] K. K. Gomes, W. Mar, W. Ko, F. Guinea, and H. C. Manoharan, *Nature* **483**, 306 (2012).
- [65] J. Dalibard, F. Gerbier, G. Juzeliūnas, and P. Öhberg, *Rev. Mod. Phys.* **83**, 1523 (2011).
- [66] B. Béri and N. R. Cooper, *Phys. Rev. Lett.* **107**, 145301 (2011).
- [67] N. Goldman, I. Satija, P. Nikolić, A. Bermudez, M. A. Martin-Delgado, M. Lewenstein, and I. B. Spielman, *Phys. Rev. Lett.* **105**, 255302 (2010).
- [68] A. Dauphin, M. Müller, and M. A. Martin-Delgado, *Phys. Rev. A* **86**, 053618 (2012).
- [69] F. Grusdt and M. Fleischhauer, arXiv:1207.3716.
- [70] J. Koch, A. A. Houck, K. L. Hur, and S. M. Girvin, *Phys. Rev. A* **82**, 043811 (2010).
- [71] A. Petrescu, A. A. Houck, and K. Le Hur, *Phys. Rev. A* **86**, 053804 (2012).
- [72] J. E. Moore, *Nature* **464**, 194 (2010).
- [73] M. Dzero, K. Sun, V. Galitski, and P. Coleman, *Phys. Rev. Lett.* **104**, 106408 (2010).
- [74] M. Dzero, K. Sun, P. Coleman, and V. Galitski, *Phys. Rev. B* **85**, 045130 (2012).
- [75] X.-L. Qi, Y.-S. Wu, and S.-C. Zhang, *Phys. Rev. B* **74**, 085308 (2006).
- [76] G. A. Fiete, V. Chua, X. Hu, M. Kargarian, R. Lundgren, A. Rüegg, J. Wen, and V. Yuzin, *Physica E* **44**, 845 (2012).
- [77] X. Qi, T. L. Hughes, and S. Zhang, *Phys. Rev. B* **78**, 195424 (2008).
- [78] C. Wu, B. A. Bernevig, and S.-C. Zhang, *Phys. Rev. Lett.* **96**, 106401 (2006).
- [79] C. Xu and J. E. Moore, *Phys. Rev. B* **73**, 045322 (2006).
- [80] A. M. Essin and V. Gurarie, *Phys. Rev. B* **85**, 195116 (2012).
- [81] Z. Y. Meng, T. C. Lang, S. Wessel, F. F. Assaad, and A. Muramatsu, *Nature* **464**, 847 (2010).
- [82] K. S. Novoselov, A. K. Geim, S. V. Morozov, D. Jiang, Y. Zhang, S. V. Dubonos, I. V. Grigorieva, and A. A. Firsov, *Science* **306**, 666 (2004).
- [83] A. H. Castro Neto, F. Guinea, N. M. R. Peres, K. S. Novoselov, and A. K. Geim, *Rev. Mod. Phys.* **81**, 109 (2009).
- [84] J. Hubbard, *Proc. R. Soc. London* **276**, 238 (1963).
- [85] P. R. Wallace, *Phys. Rev.* **71**, 622 (1947).
- [86] D. N. Sheng, Z. Y. Weng, L. Sheng, and F. D. M. Haldane, *Phys. Rev. Lett.* **97**, 036808 (2006).
- [87] S. Rachel and K. Le Hur, *Phys. Rev. B* **82**, 075106 (2010).
- [88] K. Sun, H. Yao, E. Fradkin, and S. A. Kivelson, *Phys. Rev. Lett.* **103**, 046811 (2009).
- [89] F. D. M. Haldane, *Phys. Rev. Lett.* **61**, 1029 (1988).
- [90] L. Wang, H. Shi, S. Zhang, X. Wang, X. Dai, and X. C. Xie, arXiv:1012.5163 (2010).
- [91] C. N. Varney, K. Sun, M. Rigol, and V. Galitski, *Phys. Rev. B* **82**, 115125 (2010).
- [92] C. N. Varney, K. Sun, M. Rigol, and V. Galitski, *Phys. Rev. B* **84**, 241105 (2011).
- [93] V. Juricic, A. Mesaros, R.-J. Slager, and J. Zaanen, *Phys. Rev. Lett.* **108**, 106403 (2012).
- [94] A. Medhi, V. B. Shenoy, and H. R. Krishnamurthy, *Phys. Rev. B* **85**, 235449 (2012).
- [95] D. G. Rothe, R. W. Reinthaler, C.-X. Liu, L. W. Molenkamp, S.-C. Zhang, and E. M. Hankiewicz, *New J. Phys.* **12**, 065012 (2012).
- [96] T. L. Schmidt, S. Rachel, F. von Oppen, and L. I. Glazman, *Phys. Rev. Lett.* **108**, 156402 (2012).
- [97] T. Yoshida, S. Fujimoto, and N. Kawakami, *Phys. Rev. B* **85**, 125113 (2012).
- [98] L. Wang, X. Dai, and X. C. Xie, *Eur. Phys. Lett.* **98**, 57001 (2012).
- [99] Y. Tada, R. Peters, M. Oshikawa, A. Koga, N. Kawakami, and S. Fujimoto, *Phys. Rev. B* **85**, 165138 (2012).
- [100] J. C. Budich, B. Trauzettel, and G. Sangiovanni, arXiv:1211.3059 (2012).
- [101] T. Yoshida, R. Peters, S. Fujimoto, and N. Kawakami, *Phys. Rev. B* **87**, 085134 (2013).
- [102] A. Rüegg and G. A. Fiete, *Phys. Rev. Lett.* **108**, 046401 (2012).
- [103] H.-M. Guo and M. Franz, *Phys. Rev. B* **80**, 113102 (2009).
- [104] A. Rüegg, J. Wen, and G. A. Fiete, *Phys. Rev. B* **81**, 205115 (2010).
- [105] C. Weeks and M. Franz, *Phys. Rev. B* **82**, 085310 (2010).
- [106] M. Kargarian and G. A. Fiete, *Phys. Rev. B* **82**, 085106 (2010).
- [107] X. Hu, M. Kargarian, and G. A. Fiete, *Phys. Rev. B* **84**, 155116 (2011).
- [108] A. Kitaev, *Annals of Physics* **303**, 2 (2003).
- [109] A. Kitaev, *Annals of Physics* **321**, 2 (2006).
- [110] M. A. N. Araújo, E. V. Castro, and P. D. Sacramento, *Phys. Rev. B* **87**, 085109 (2013).
- [111] J. Goryo and N. Maeda, *J. Phys. Soc. Jpn.* **80**, 044707 (2011).
- [112] D. Cocks, P. P. Orth, S. Rachel, M. Buchhold, K. Le Hur, and W. Hofstetter, *Phys. Rev. Lett.* **109**, 205303 (2012).
- [113] Q. Niu, D. J. Thouless, and Y.-S. Wu, *Phys. Rev. B* **31**, 3372 (1985).
- [114] D. Xiao, M.-C. Chang, and Q. Niu, *Rev. Mod. Phys.* **82**, 1959 (2010).
- [115] W.-Y. Hsiang and D.-H. Lee, *Phys. Rev. A* **64**, 052101 (2001).
- [116] G. E. Volovik, *The Universe in a Helium Droplet* (Clarendon Press, Oxford, 2003).
- [117] D. N. Sheng, L. Balents, and Z. Wang, *Phys. Rev. Lett.* **91**, 116802 (2003).
- [118] G. W. Semenoff, *Phys. Rev. Lett.* **53**, 2449 (1984).
- [119] L. Fu and C. L. Kane, *Phys. Rev. B* **74**, 195312 (2006).
- [120] X. G. Wen, *Phys. Rev. B* **41**, 12838 (1990).
- [121] X. G. Wen, *Int. J. Mod. Phys. B* **6**, 1711 (1992).
- [122] C. L. Kane and M. P. A. Fisher, *Phys. Rev. Lett.* **68**, 1220 (1992).
- [123] M. Onoda, Y. Avishai, and N. Nagaosa, *Phys. Rev. Lett.* **98**, 076802 (2007).
- [124] T. Neupert, L. Santos, S. Ryu, C. Chamon, and C. Mudry, *Phys. Rev. B* **84**, 165107 (2011).
- [125] M. Hohenadler, T. C. Lang, and F. F. Assaad, *Phys. Rev. Lett.* **106**, 100403 (2011), erratum **109**, 229902(E) (2012).
- [126] M. Hohenadler, Z. Y. Meng, T. C. Lang, S. Wessel, A. Muramatsu, and F. F. Assaad, *Phys. Rev. B* **85**, 115132 (2012).
- [127] F. F. Assaad, M. Bercx, and M. Hohenadler, *Phys. Rev. X* **3**, 011015 (2013).

- (2013).
- [128] C. Griset and C. Xu, Phys. Rev. B **85**, 045123 (2012).
- [129] D. Zheng, G.-M. Zhang, and C. Wu, Phys. Rev. B **84**, 205121 (2011).
- [130] Y. Yamaji and M. Imada, Phys. Rev. B **83**, 205122 (2011).
- [131] W. Wu, S. Rachel, W.-M. Liu, and K. Le Hur, Phys. Rev. B **85**, 205102 (2012).
- [132] S.-L. Yu, X. C. Xie, and J.-X. Li, Phys. Rev. Lett. **107**, 010401 (2011).
- [133] J. C. Budich, R. Thomale, G. Li, M. Laubach, and S.-C. Zhang, Phys. Rev. B **86**, 201407 (2012).
- [134] A. Liebsch, Phys. Rev. B **83**, 035113 (2011).
- [135] J. Wen, M. Kargarian, A. Vaezi, and G. A. Fiete, Phys. Rev. B **84**, 235149 (2011).
- [136] M. Mardani, M.-S. Vaezi, and A. Vaezi, arXiv:1111.5980 (2011).
- [137] A. Vaezi, M. Mashkooori, and M. Hosseini, Phys. Rev. B **85**, 195126 (2012).
- [138] D.-H. Lee, Phys. Rev. Lett. **107**, 166806 (2011).
- [139] S. Sorella, Y. Otsuka, and S. Yunoki, Sci. Rep. **2**, 992 (2012).
- [140] M. Hohenadler and F. F. Assaad, Phys. Rev. B **85**, 081106 (2012), erratum **86**, 199901(E) (2012).
- [141] R. S. K. Mong, A. M. Essin, and J. E. Moore, Phys. Rev. B **81**, 245209 (2010).
- [142] M. Campostrini, M. Hasenbusch, A. Pelissetto, and E. Vicari, Phys. Rev. B **74**, 144506 (2006).
- [143] T. Grover and A. Vishwanath, arXiv:1206.1332 (2012).
- [144] V. Anisimov, I. Nekrasov, D. Kondakov, T. Rice, and M. Sigrist, Eur. Phys. J. B **25**, 191 (2002).
- [145] A. Liebsch, Phys. Rev. Lett. **91**, 226401 (2003).
- [146] A. Koga, N. Kawakami, T. M. Rice, and M. Sigrist, Phys. Rev. Lett. **92**, 216402 (2004).
- [147] R. Arita and K. Held, Phys. Rev. B **72**, 201102 (2005).
- [148] H. Guo, S. Feng, and S.-Q. Shen, Phys. Rev. B **83**, 045114 (2011).
- [149] J. He, Y.-H. Zong, S.-P. Kou, Y. Liang, and S. Feng, Phys. Rev. B **84**, 035127 (2011).
- [150] J. He, B. Wang, and S.-P. Kou, Phys. Rev. B **86**, 235146 (2012).
- [151] T. Neupert, L. Santos, S. Ryu, C. Chamon, and C. Mudry, Phys. Rev. Lett. **108**, 046806 (2012).
- [152] I. F. Herbut, Phys. Rev. Lett. **97**, 146401 (2006).
- [153] C. Honerkamp, Phys. Rev. Lett. **100**, 146404 (2008).
- [154] Y. Ran, A. Vishwanath, and D.-H. Lee, Phys. Rev. Lett. **101**, 086801 (2008).
- [155] R. Nandkishore, M. A. Metlitski, and T. Senthil, Phys. Rev. B **86**, 045128 (2012).
- [156] C. Wu and S.-C. Zhang, Phys. Rev. Lett. **93**, 036403 (2004).
- [157] C. Weeks and M. Franz, Phys. Rev. B **81**, 085105 (2010).
- [158] Q. Liu, H. Yao, and T. Ma, Phys. Rev. B **82**, 045102 (2010).
- [159] J. Wen, A. Rüegg, C.-C. J. Wang, and G. A. Fiete, Phys. Rev. B **82**, 075125 (2010).
- [160] Y. Zhang, Y. Ran, and A. Vishwanath, Phys. Rev. B **79**, 245331 (2009).
- [161] M. W. Young, S.-S. Lee, and C. Kallin, Phys. Rev. B **78**, 125316 (2008).
- [162] B. A. Bernevig and S.-C. Zhang, Phys. Rev. Lett. **96**, 106802 (2006).
- [163] E. Tang, J.-W. Mei, and X.-G. Wen, Phys. Rev. Lett. **106**, 236802 (2011).
- [164] K. Sun, Z. Gu, H. Katsura, and S. Das Sarma, Phys. Rev. Lett. **106**, 236803 (2011).
- [165] T. Neupert, L. Santos, C. Chamon, and C. Mudry, Phys. Rev. Lett. **106**, 236804 (2011).
- [166] M. Levin, F. J. Burnell, M. Koch-Janusz, and A. Stern, Phys. Rev. B **84**, 235145 (2011).
- [167] A. M. Läuchli, Z. Liu, E. J. Berholtz, and R. Moessner, arXiv:1207.6094 (2012).
- [168] N. Regnault and B. A. Bernevig, Phys. Rev. X **1**, 021014 (2011).
- [169] Y.-H. Wu, J. K. Jain, and K. Sun, Phys. Rev. B **86**, 165129 (2012).
- [170] T. Scaffidi and G. Möller, Phys. Rev. Lett. **109**, 246805 (2012).
- [171] G. Y. Cho and J. E. Moore, Annals of Physics **326**, 1515 (2011).
- [172] M. Levin and A. Stern, Phys. Rev. B **86**, 115131 (2012).
- [173] Y.-M. Lu and Y. Ran, Phys. Rev. B **85**, 165134 (2012).
- [174] D. Ferraro and G. Viola, arXiv:1112.5399 (2011).
- [175] R. Roy, arXiv:1208.2055 (2012).
- [176] P. Nikolić, J. Phys.: Condensed Matter **25**, 025602 (2013).
- [177] P. Nikolić, arXiv:1206.1055 (2012).
- [178] A. G. Grushin, T. Neupert, C. Chamon, and C. Mudry, Phys. Rev. B **86**, 205125 (2012).
- [179] B. Béri and N. R. Cooper, Phys. Rev. Lett. **108**, 206804 (2012).
- [180] T. Liu, C. Repellin, B. A. Bernevig, and N. Regnault, arXiv:1206.2626 (2012).
- [181] B. Béri and N. R. Cooper, Phys. Rev. Lett. **106**, 156401 (2011).
- [182] J. Voit, Rep. Prog. Phys. **57**, 977 (1995).
- [183] G. Tkachov and E. M. Hankiewicz, Phys. Status Solidi **250**, 215 (2013).
- [184] Y. Tanaka and N. Nagaosa, Phys. Rev. Lett. **103**, 166403 (2009).
- [185] G. Autès and O. V. Yazyev, physica status solidi (RRL) **7**, 151 (2013).
- [186] X.-L. Qi, T. L. Hughes, and S.-C. Zhang, Nat. Phys. **4**, 273 (2008).
- [187] J. C. Budich, F. Dolcini, P. Recher, and B. Trauzettel, Phys. Rev. Lett. **108**, 086602 (2012).
- [188] A. Medhi and V. B. Shenoy, J. Phys: Condens. Matter **24**, 355001 (2012).
- [189] A. V. Moroz, K. V. Samokhin, and C. H. W. Barnes, Phys. Rev. Lett. **84**, 4164 (2000).
- [190] A. Iucci, Phys. Rev. B **68**, 075107 (2003).
- [191] Y. A. Bychkov and E. I. Rashba, J. Phys. C: Solid State Phys. **17**, 6039 (1984).
- [192] J. Maciejko, C. Liu, Y. Oreg, X.-L. Qi, C. Wu, and S.-C. Zhang, Phys. Rev. Lett. **102**, 256803 (2009).
- [193] J. Maciejko, Phys. Rev. B **85**, 245108 (2012).
- [194] F. Crépin, J. C. Budich, F. Dolcini, P. Recher, and B. Trauzettel, Phys. Rev. B **86**, 121106 (2012).
- [195] M. Kharitonov, Phys. Rev. B **86**, 165121 (2012).
- [196] H. J. Schulz, Phys. Rev. Lett. **71**, 1864 (1993).
- [197] D. Soriano and J. Fernández-Rossier, Phys. Rev. B **82**, 161302 (2010).
- [198] H. Feldner, Z. Y. Meng, T. C. Lang, F. F. Assaad, S. Wessel, and A. Honecker, Phys. Rev. Lett. **106**, 226401 (2011).
- [199] D. J. Luitz, F. F. Assaad, and M. J. Schmidt, Phys. Rev. B **83**, 195432 (2011).
- [200] M. J. Schmidt, Phys. Rev. B **86**, 075458 (2012).
- [201] B. Braunecker, C. Bena, and P. Simon, Phys. Rev. B **85**, 035136 (2012).
- [202] X.-L. Qi, Y.-S. Wu, and S.-C. Zhang, Phys. Rev. B **74**, 045125 (2006).
- [203] V. Gurarie, Phys. Rev. B **83**, 085426 (2011).
- [204] A. Furusaki and N. Nagaosa, Phys. Rev. Lett. **72**, 892 (1994).
- [205] J. Yuan, J.-H. Gao, W.-Q. Chen, F. Ye, Y. Zhou, and F.-C. Zhang, Phys. Rev. B **86**, 104505 (2012).
- [206] R. R. P. Singh and R. T. Scalettar, Phys. Rev. Lett. **66**, 3203 (1991).
- [207] M. Hohenadler and F. F. Assaad, (unpublished).
- [208] Z. Wang and B. Yan, arXiv:1207.7341 (2012).
- [209] K. Ishikawa and T. Matsuyama, Nucl. Phys. B **280**, 523 (1987).
- [210] S. Kourtis, J. W. F. Venderbos, and M. Daghofer, Phys. Rev. B **86**, 235118 (2012).
- [211] T. Fukui and Y. Hatsugai, Phys. Rev. B **75**, 121403 (2007).
- [212] S.-S. Lee and S. Ryu, Phys. Rev. Lett. **100**, 186807 (2008).
- [213] K. Ishikawa and T. Matsuyama, Z. Physik C **33**, 41 (1986).
- [214] H. So, Prog. Theor. Phys. **74**, 585 (1985).
- [215] Z. Wang, X.-L. Qi, and S.-C. Zhang, Phys. Rev. Lett. **105**, 256803 (2010).
- [216] L. Wang, H. Jiang, X. Dai, and X. C. Xie, Phys. Rev. B **85**, 235135 (2012).
- [217] T. Fukui, Y. Hatsugai, and H. Suzuki, J. Phys. Soc. Jpn. **74**, 1674 (2005).
- [218] A. M. Essin and V. Gurarie, Phys. Rev. B **84**, 125132 (2011).
- [219] V. Gurarie and A. M. Essin, arXiv:1301.3941 (2013).
- [220] Z. Wang and S.-C. Zhang, Phys. Rev. B **86**, 165116 (2012).
- [221] J. C. Budich and B. Trauzettel, arXiv:1207.1104 (2012).
- [222] S. R. Manmana, A. M. Essin, R. M. Noack, and V. Gurarie, Phys.

- Rev. B **86**, 205119 (2012).
- [223] A. Go, W. Witczak-Krempa, G. S. Jeon, K. Park, and Y. B. Kim, Phys. Rev. Lett. **109**, 066401 (2012).
- [224] Z. Wang and S.-C. Zhang, Phys. Rev. X **2**, 031008 (2012).
- [225] Z. Wang, X.-L. Qi, and S.-C. Zhang, Phys. Rev. B **85**, 165126 (2012).
- [226] A. Georges, G. Kotliar, W. Krauth, and M. J. Rozenberg, Rev. Mod. Phys. **68**, 13 (1996).
- [227] L. Wang, X. Dai, and X. C. Xie, Phys. Rev. B **84**, 205116 (2011).
- [228] X.-L. Qi and S.-C. Zhang, Phys. Rev. Lett. **101**, 086802 (2008).
- [229] D.-H. Lee, G.-M. Zhang, and T. Xiang, Phys. Rev. Lett. **99**, 196805 (2007).
- [230] J. He, Y.-X. Zhu, Y.-J. Wu, L.-F. Liu, Y. Liang, and S.-P. Kou, arXiv:1210.0266 (2012).
- [231] A. Rüegg and C. Lin, Phys. Rev. Lett. **110**, 046401 (2013).
- [232] W. P. Su, J. R. Schrieffer, and A. J. Heeger, Phys. Rev. Lett. **42**, 1698 (1979).
- [233] U. Schollwöck, Rev. Mod. Phys. **77**, 259 (2005).
- [234] G. Vidal, J. I. Latorre, E. Rico, and A. Kitaev, Phys. Rev. Lett. **90**, 227902 (2003).
- [235] A. Kitaev and J. Preskill, Phys. Rev. Lett. **96**, 110404 (2006).
- [236] M. Levin and X.-G. Wen, Phys. Rev. Lett. **96**, 110405 (2006).
- [237] S. Depenbrock, I. P. McCulloch, and U. Schollwöck, Phys. Rev. Lett. **109**, 067201 (2012).
- [238] H.-C. Jiang, Z. Wang, and L. Balents, Nat. Phys. **8**, 902 (2012).
- [239] H. Li and F. D. M. Haldane, Phys. Rev. Lett. **101**, 010504 (2008).
- [240] A. M. Turner, Y. Zhang, and A. Vishwanath, Phys. Rev. B **82**, 241102 (2010).
- [241] X.-L. Qi, H. Katsura, and A. W. W. Ludwig, Phys. Rev. Lett. **108**, 196402 (2012).
- [242] M. P. Zaletel, R. S. K. Mong, and F. Pollmann, arXiv:1211.3733 (2012).